Surveys in Geophysics
May 2014, Volume 35, Issue 3, Pages 681-722
http://dx.doi.org/10.1007/s10712-013-9244-0

The original publication is available at http://www.springerlink.com

Sea Surface Salinity Observations from Space with the SMOS Satellite: A New Means to Monitor the Marine Branch of the Water Cycle

Nicolas Reul[*, 1, 2], Severine Fournier[1], Jaqueline Boutin[3], Olga Hernandez[3], Christophe Maes[5], Bertrand Chapron[1], Gaël Alory[5], Yves Quilfen[1], Joseph Tenerelli[4], Simmon Morisset[3], Yann Kerr[6], Susanne Mecklenburg[7], Steven Delwart[7]

[1] Laboratoire d'Océanographie Spatiale, Institut Français de recherche et d'Exploitation de la Mer, Centre Bretagne BP 70, 29280, Plouzané, France
[2] Centre Méditerranée, Zone Portuaire de Brégaillon, BP 330, 83507, La Seyne-sur-Mer Cedex, France
[3] Laboratoire d'Océanographie et du Climat: Expérimentation et Approches Numériques, UMR 7159 CNRS/UPMC/IRD/MNHN, Paris, France
[5] LEGOS, OMP, CNAP, Université de Toulouse, Toulouse, France
[4] CLS-Radar Division, Bâtiment Le Ponant, Avenue La Pérouse, Technopôle Brest-Iroise, 29280, Plouzané, France
[6] CESBIO, Toulouse, France
[7] ESA-ESRIN, Frascatti, Italy

*: Corresponding author : Nicolas Reul, email address : nreul@ifremer.fr

Abstract:

While it is well known that the ocean is one of the most important component of the climate system, with a heat capacity 1,100 times greater than the atmosphere, the ocean is also the primary reservoir for freshwater transport to the atmosphere and largest component of the global water cycle. Two new satellite sensors, the ESA Soil Moisture and Ocean Salinity (SMOS) and the NASA Aquarius SAC-D missions, are now providing the first space-borne measurements of the sea surface salinity (SSS). In this paper, we present examples demonstrating how SMOS-derived SSS data are being used to better characterize key land–ocean and atmosphere–ocean interaction processes that occur within the marine hydrological cycle. In particular, SMOS with its ocean mapping capability provides observations across the world's largest tropical ocean fresh pool regions, and we discuss from intraseasonal to interannual precipitation impacts as well as large-scale river runoff from the Amazon–Orinoco and Congo rivers and its offshore advection. Synergistic multi-satellite analyses of these new surface salinity data sets combined with sea surface temperature, dynamical height and currents from altimetry, surface wind, ocean color, rainfall estimates, and in situ observations are shown to yield new freshwater budget insight. Finally, SSS observations from the SMOS and Aquarius/SAC-D sensors are combined to examine the response of the upper ocean to tropical cyclone passage including the potential role that a freshwater-induced upper ocean barrier layer may play in modulating surface cooling and enthalpy flux in tropical cyclone track regions.

Keywords: Sea surface salinity ; SMOS satellite ; Passive microwave remote sensing ; Oceanic freshwater cycle

1. Introduction

Salinity is known to play an important role in the dynamics of the ocean's thermohaline overturning circulation and in large-scale atmosphere–ocean climate signals such as the El Nino Southern Oscillation (ENSO), and is the key freshwater tracer within the oceanic component of the global hydrologic cycle, a branch that comprises most of the global precipitation and evaporation as well as the river runoff (Schmitt 2008). Multi-decadal sea surface salinity (SSS) trends have been documented in tropical and high latitudes and associated with signatures of evaporation or precipitation variation that are consistent with global warming scenarios (e.g., Dickson et al. 2002; Gordon and Guilivi 2008; Morrow et al. 2008; Cravatte et al. 2009; Yu 2011; Durack et al. 2012; Terray et al. 2011). These studies highlight the need for well-sampled SSS time series both for monitoring the change and to improve basic understanding of the respective roles of the atmosphere and ocean dynamics, thermodynamics, air–sea interaction, and land-ocean interaction in the global water cycle context.

Our basic knowledge of the global SSS distribution is derived from the compilations of all available oceanographic data collected over time (e.g. Boyer and Levitus, 2002). The SSS in situ observing system has expanded significantly during the last decade due mostly to the full deployment of the Argo profiling float array, and now provides a monthly SSS estimate on a grid of roughly 300-400 km^2. Notwithstanding these recent gains, this sampling density is still too sparse to resolve climatologically important intraseasonal, seasonal, and interannual to decadal signals at the 300 km spatial scale within which SSS is known to vary significantly (Lagerloef et al, 2010). The recent launch of the ESA/SMOS (Soil Moisture and Ocean Salinity, see Kerr et al., 2010; Font et al., 2010) and NASA/Aquarius SAC-D (Lagerloef et al., 2008; Lagerloef et al., 2012) mission satellites represent contributions towards filling this gap using passive microwave remote sensing.

Salinity remote sensing is based on measurement of sea surface microwave emission at the lower end of the microwave spectrum and from a surface skin layer having a thickness of *O*(1 cm). This emission depends partly on the dielectric constant of sea water, which in turn can be related to salinity and temperature. Thus, given sea surface temperature (SST), theory predicts some ability to invert SSS information. In practice however, numerous additional external factors (extra-terrestrial sources, atmosphere, ionosphere and surface roughness) also contribute to the satellite-observed emission and these must be corrected to allow accurate ocean salinity estimates. The SMOS and Aquarius sensors are both ocean microwave radiometers operating at a frequency of ~1.4 GHz (L-band, wavelength of 21 cm), a band chosen for the relatively strong sensitivity to change in salinity and because this is a transmission-free, or protected, frequency. An additional and important benefit for this choice is minimization of atmospheric signal contributions.

Based on observed SSS variability and need to better resolve it, the satellite missions aim to produce salinity estimates with an accuracy of 0.1–0.2 over the so-called Global Ocean Data Assimilation Experiment (GODAE) scales of 100 km, one month or 200 km, and 10 days. This is a challenging objective for several reasons. First, the sensitivity of L-band brightness temperatures to variations in SSS is on average 0.5 degK per salinity unit. This sensitivity is very weak given that spatial and temporal variability in open-ocean SSS does not exceed several units and that the instrument noise is typically 2–5 degK. Second, there are many geophysical sources of brightness at L-band that corrupt the salinity signal, and correction models for these factors have uncertain accuracy. Moreover, the technical approach developed in order to achieve adequate radiometric accuracy and spatio-temporal resolution for SMOS is polarimetric interferometric radiometry, the first such spaceborne system. The complex SMOS image reconstruction data processing includes contamination by different errors and induces residual inaccuracies in SSS estimates. Finally, there is significant radio frequency interference emanating from sources along the many coastlines that contaminate data collected over many ocean regions. Nevertheless, much work at ESA SMOS Level 2 expert centers and the CNES/IFREMER Centre Aval de Traitement des Données SMOS (CATDS) has addressed these issues, leading to the first global satellite SSS estimates (Font et al. 2012, Reul et al. 2012, Boutin et al. 2012a).

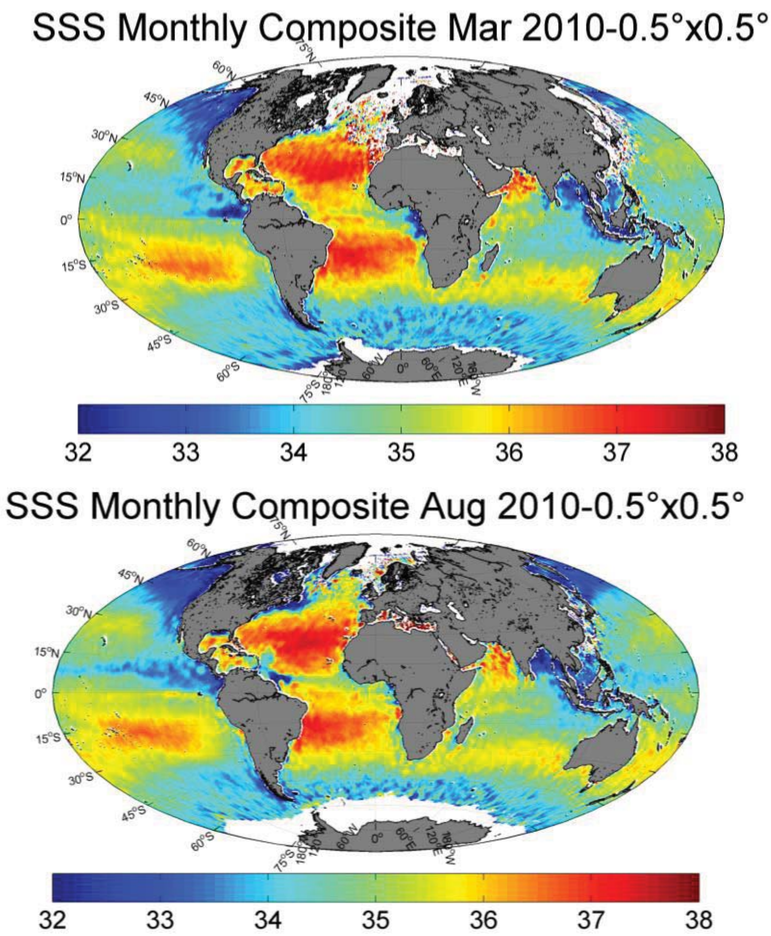

Figure. 1 *Monthly composites of the sea surface salinity at a spatial resolution of 0.5°x0.5° deduced from SMOS data (CATDS v2) for the months of March (top) and August (bottom) 2010.*

Two examples of monthly composite SMOS SSS maps are shown in Figure 1. They show salient basin scale features, including the elevated salinity in the Atlantic relative to the other basins, and the general correspondence of lower SSS with known river runoff and tropical precipitation regions. SMOS data validation efforts using *in situ* observations reveal an overall SSS accuracy on the order of 0.3 (Boutin et al., 2012a; Reul et al., 2012; Bank et al., 2012; Font et al., 2013), but with degraded quality at high latitudes partly because of reduced sensitivity in colder waters. While further improvements are in progress, many interesting features of the global SSS could be already evidenced.

This paper reviews preliminary results addressing several key applications of these new satellite SSS data. Given the reduced SMOS sensitivity in colder waters, the focus in on tropical ocean data where SMOS measurements have proven to be the most accurate. We also attempt to highlight combined use of other satellite and *in situ* observations (altimetry, SST, ocean color, river discharge, evaporation, precipitation). It is shown that these new data are proving useful in the monitoring of intraseasonal to interannual variability across major Tropical freshwater pools of the world ocean. SMOS-detected SSS freshening events within intense precipitation zones (e.g., the Inter-Tropical Convergence Zone) are also shown to provide promising new information related to the ocean surface response to rainfall. Finally, SMOS SSS data are used to address interactions between wind-driven phenomena, such as upwelling and Tropical cyclones, and some of the world largest Fresh pools. The datasets used in these cases are described in Section 2. SMOS monitoring capabilities for the major tropical river plumes are given in Section 3. In sections 4 and 5, we illustrate rain impacts detected in SMOS SSS data then their application improved understanding of freshwater pools interaction with the atmosphere. Conclusions and perspectives are given in section 6.

2. Data

A range of satellite and *in situ* datasets are used in the present study with focus on the years 2010-2011 following the SMOS launch date. The data products are described below.

2.1 SMOS SSS data

SMOS (Soil Moisture and Ocean Salinity) is the European Space Agency (ESA)'s water mission (Kerr et al. 2010; Mecklenburg et al. 2012), an Earth Explorer Opportunity

Mission approved under the Living Planet Program. SMOS was launched in November 2009 and the technical approach developed to achieve adequate radiometric accuracy, as well as spatial and temporal resolution compromising between land and ocean science requirements, is polarimetric interferometric radiometry (Ruf et al. 1988; Font et al. 2010) at L-band (frequency of ~1.4 GHz). ESA produces so-called Level 2 SSS, or L2 products which correspond to instantaneous SSS retrievals under the satellite swath.

Table 1: Summary of characteristics of CATDS-CEC SSS level 3 products

	CEC IFREMER	CEC LOCEAN
SSS retrievalmethod	SSS retrieved from first Stokes parameter (Reul and Tenerelli 2011)	SSS retrieved from polarized Tbs along dwell-lines using an iterative retrieval (see ESA L2OS ATBD)
Region of the instrument field of View (FOV) considered for SSS retrieval	Alias Free Field of View only	Alias Free Field of View (AFFOV) and extended AFFOV along dwell lines with at least 130 Tb in AFFOV (~ +/-300km from the swath center)
Tb sortings	Determined from interorbit consistency in incidence angles classes and thresholding	Determined from consistency along dwell lines as reported in ESA level 2 products
Galactic model	Geometrical optics model	Kirchoff Approx. scattering at 3m/s
Roughness/foammodels	Empirical adjustment of Tb dependencies to wind speed	Empirical adjustment of parameters in roughness model and foam coverage models (Yin et al. 2012)
Calibration	Single Ocean Target Transformation (OTT) + daily 5°x5° adjustment wrt World Ocean 2001 SSS climatology	Variable OTT (every 2 weeks synchronised with Noise Injection Radiometer as defined in ESA reprocessing)
Average	Simple average	Average weighted by theoretical error on retrieved SSS and spatial

		resolution

In the present study, level 2 SMOS SSS are from the first SMOS/ESA annual reprocessing campaign in which ESA level 1 v5.04 and level 2 v5.50 processors havebeen used. In these versions, significant improvements with respect to the flaws discovered in the first products (e.g. Reul et al., 2012) have been implemented (see a complete description in the Algorithm TheoreticalBasis Document (ATBD) available at http://www.argans.co.uk/smos/docs/deliverables/). Nevertheless, accuracy of these instantaneous SSS retrievals is rather low (~0.6-1.7 unit) and space-time averaging of the Level 2 products is needed (so-called Level 3 SSS) to decrease the noise level in the retrievals.

Here we used two types of composite SSS level 3 products generated in laboratories participating to the Expertise Center of the Centre Aval de Traitement des Données SMOS (CATDS, http://www.catds.fr), which is the french ground segment for the SMOS data. These products are built either from ESA level 1 products (Reul and Tenerelli, 2011) or from ESA level 2 products (Boutin et al, 2012b).

These research products aim at assessing the quality of SMOS operational products (ESA level 2 and CATDS-OP level 3) and at studying new processings to be implemented in the future in operational chains. Main characteristics of these products are detailed in Table 1. CEC-IFREMER products have been used in section 3 & 5, CEC-LOCEAN products in section 4.

Overall accuracy of the 10-days composite products at 25 km resolution is on the order of 0.3 practical salinity unit in the tropical oceans (Reul and Tenerelli, 2011). Note thatsalinity computations are based on the Practical Salinity Scale PSS-78, and reported with no units (United Nations Educational, Scientific and Cultural Organization, 1985).

2.2 Ocean Surface Currents

Here we used the 1/3° resolution global surface current products from Ocean Surface Current Analyses Realtime (OSCAR) (Bonjean and Lagerloef, 2002; http://www.oscar.noaa.gov), directly calculated from satellite altimetry and ocean vector winds.

The OSCAR data processing system calculates sea surface velocities from satellite altimetry (AVISO), vector wind fields (QuikSCAT), as well as from sea surface temperature (Reynolds-Smith) using quasi-steady geostrophic, local wind-driven, and thermal wind dynamics. Near real time velocities are calculated on both a 1°x1° and 1/3°x1/3° grid on a ~5 day time base over the global ocean. Surface currents are provided on the OSCAR website (http://www.oscar.noaa.gov) starting from 1992 along with validations with drifters and moorings. The 1/3° resolution is available for ftp download through ftp://ftp.esr.org/pub/datasets/SfcCurrents/ThirdDegree.

2.3 Rain, Evaporation and River Discharge data

To estimate the rain-rate over the oceans, we used three different satellite products.

One is the monthly TRMM Composite Climatology (TCC) of surface precipitation based on 13 years of data from the Tropical Rainfall Measuring Mission (TRMM). The TCC takes advantage of the information from multiple estimates of precipitation from TRMM to construct mean value maps over the tropics (36°N - 36°S) for each month of the year at 0.5° latitude-longitude resolution. The first-time use of both active and passive microwave instruments on board TRMM has made it the foremost satellite for the study of precipitation in the tropics and has led to a better understanding of the underlying physics and distribution of precipitation in this region. The products are available at NASA Goddard Space Flight Center Global Change Master Directory (http://gcmd.nasa.gov).

The second type of satellite rain rate estimates that we used in the present study are the so-called 'TRMM and Other Satellites' (3B42) products, obtained through the NASA/Giovanni server (http://reason.gsfc.nasa.gov/OPS/Giovanni).The 3B42 estimates are 3-hourly at a spatial resolution of 0.25° with spatial extentcovering a global belt (−180°W to 180° E) extending from50°S to 50°N latitude. The major inputs into the 3B42 algorithm are IR data from geostationary satellites and Passive Microwave data from the TRMM microwave imager (TMI), special sensor microwave imager (SSM/I), Advanced Microwave Sounding Unit (AMSU) and Advanced Microwave Sounding Radiometer-Earth Observing System (AMSR-E).

The Special Sensor Microwave Imager (SSM/I) F16 and F17 orbits cross SMOS orbits within -20 min and +40 min. Hence, numerous SMOS level 2 are collocated with SSMI rain rates (RR) within this range of time. In addition to the TRMM 3B42 products, we therefore used SSM/Is datasets to perform co-locations between SMOS SSS and rain estimates. SSM/Is RR version 7 were used and downloaded from http://www.remss.com.

The evaporation (*E*) data set was taken from the Version 3 products of the Objectively Analyzed air-sea Fluxes (OAFlux) project (Yu and Weller, 2007).

Finally the discharge data for the Amazon, Orinoco and Congo rivers were obtained from the Environmental Research Observatory (ORE) HYBAM (Geodynamical, hydrological and biogeochemical control of erosion/alteration and material transport in the Amazon basin) website.

2.4 Ocean Color products

To study the spatio-temporal coherency between SSS signals from some major tropical river plumes and ocean color properties, we used the level-3 daily, 4-km resolution estimates of the absorption coefficient ofcolored detrital matter (CDM) at 443 nm. These products processed and distributed by ACRI-ST GlobColour service, are supported by the EU FP7 MyOcean2 and the ESA GlobColour Projects, using ESA ENVISAT MERIS data, NASA MODIS and SeaWiFS data. These products have been averaged at the SMOS L3 product 0.25° resolution, with a 10-days running mean.

2.5 In situ data

Salinity measurements from Argo floats are provided by the Coriolis data centre (http://www.coriolis.eu.org/). The upper ocean salinity values recorded between 4m and 10m depth will be referred to as Argo SSS following Boutin et al. (2012b).

Global SSS maps are derived from delayed time quality checked in situ measurements (Argo and ship) by IFREMER/LPO, Laboratoire de physique des oceans, using the In Situ Analysis System (ISAS) optimal interpolation (D7CA2S0 re-analysis product) (see a method description on http://wwz.ifremer.fr/lpo/SO-Argo-France/Products/Global-Ocean-T-S/Monthly-fields-2004-2010 and in (Gaillard et al., 2009)). The choice for the time and space scales used in that method results from a compromise between what is known of ocean time and space scales and what can actually be resolved with the Argo array (3°, 10 days); two length-scales are considered: the first one is isotropic and equal to 300 km, the second one is set equal to 4 times the average Rossby radius of deformation of the area. As a result, we expect these maps being smoother, especially in tropical areas, than SMOS SSS maps averaged over 0.25°x0.25° or 1° ×1°.

3. SMOS monitoring of the Major Tropical Atlantic River Plumes

Rivers are important variables in oceanography as their fresh water affects SSS and the buoyancy of the surface layer, and they represent a source of materials exotic to the ocean and important to biological activity. Obviously, they are key hydrologic components of the fresh water exchanges between land and ocean. Despite this importance, tracing major tropical river water (e.g. Amazon, Congo, Ganges) over large distances has not been straightforward previously principally because of a lack of SSS observations. Tracing those very large rivers over great distances now become an important endeavor, as sufficient data are available from surface salinity sensors placed aboard satellites.

Occurrence of patches of low surface salinity (< 35 practical salinity units) in the Tropical Atlantic Ocean is closely related to the presence of the mouths of the world's largest rivers in terms of fresh-water discharge (e.g. Amazon, Congo,Orinoco) and their subsequent spreading of fresh water by the upper ocean circulation. Another key fresh water source here is the Inter Tropical Convergence Zone (ITCZ), associated with relatively intense precipitation that migrates latitudinally over the tropical Atlantic throughout the year (Binet and Marchal 1993). One of these major low salinity pools is formed by the Amazon and Orinoco river plumes spreading offshore from the South America north-eastern coasts, and influencing a large fraction of the western tropical North Atlantic (Neumann, 1969; Lentz 1995; Muller-Karger et al. 1988; Dessier and Donguy, 1994). The Gulf of Guinea, situated in the North-Eastern Equatorial Atlantic (NEEA) is also an important location for the fresh water budget in the tropical Atlantic. It is a region of intense precipitation with as much as 30 cm of rain falling per month during the rainy season (Yoo and Carton [1988]). Furthermore, into this area flows the Congo River, the largest fresh water input to any eastern ocean boundary. These large-scale low salinity 'lenses' at the Tropical Atlantic surface can be traced over distances ranging from several hundreds up to thousands of kilometers in the upper ocean. They are characterized by very distinct and in general strong seasonally varying spatial extents.

3.1 Amazon and Orinoco River Plume monitoring

The Amazon is the world's largest river in terms of fresh water discharge (Milliman and Meade, 1983; Perry et al. 1996). It drains a large fraction of the South American continent, discharging on average $1.55\pm0.13 \times 10^5$ m^3s^{-1} of fresh water into the equatorial Atlantic Ocean (Perry et al.1996).This is about 15% of the estimated global river discharge on an annual basis. The Amazon River is by far the largest single source of terrestrial fresh water to the ocean and contributes about 30% of total river discharge to the Atlantic Ocean (Wisser et al., 2010). The structure of the Amazon plume is strongly influenced by a variety of physical processes which are present on the northern Brazilian shelf: the North Brazil Current (Flagg et al., 1986; Richardson and McKee, 1984), trade winds (Hellerman and Rosenstein, 1983) and strong currents associated to the tide (Nittrouer and Demaster, 1986). These physical processes play a very significant role in the dispersal and spreading of Amazon discharge (fresh water and suspended sediment) on the northern continental shelf of South America.

Previous studies have shown that Amazon Plume water can be traced offshore and northwestward along the north Brazilian coast, covering most of the continental shelf from 11°S to 5°N (Muller-Karger et al. 1988, 1995) into the Caribbean (e.g. Steven and Brooks 1972; Froelich et al.1978; Hellweger and Gordon, 2002; Cherubin and Richardson,2007), and over 1000 km eastward into the North Atlantic depending on the season. Beyond this region, the Amazon's water has been traced northwestward into the Caribbean Sea and eastward in the North Atlantic (Muller-Karger et al. 1988, 1995; Johns et al., 1990; Hellweger and Gordon, 2002). Hydrographic surveys by Lentz and Limeburner (1995) revealed that the Amazon Plume over the shelfis typically 3-10m thick and between 80 and >200 km wide. Beyond the shelf, fresh water within the plume gradually attenuates with depth as it travels away from the source, with a penetration depth of 40m to 45m as far as 2600 km offshore (Hellweger and Gordon, 2002; Hu et al., 2004).
Both chlorophyll (Chl) concentration and primary productivity are greatest in the river plume-ocean transition zone, where the bulk of heavy sediments are deposited (Smith and Demaster, 1996). The combination of riverine nutrient input and increased irradiance availability creates a highly productive transition zone, the location of which varies with the discharge from the river. High phytoplankton biomass and productivity of over 25 mg Chl-a $m^{-3}$and 8 g Cm^{-2} d^{-1}, respectively, are found in this transition region (Smith and Demaster, 1996). Because ofthis, the North Brazil shelf acts as a significant sink for atmospheric CO_2 (Ternon et al., 2000).

The north western Tropical Atlantic is also an area where another major river in the world, the Orinoco, enters the ocean. The Orinoco River originates in the southern part of Venezuela, and discharges waters from about 31 major and 2000 minor tributaries into the western tropical Atlantic. These waters are most of the time transported into the southeastern Caribbean sea and during the rainy season a larger but unquantified fraction of the plume also flows east around Trinidad and Tobago into the Caribbean. The Orinoco is considered to be the third largest river in the world in terms of volumetric discharge (after the Amazon and the Congo), discharging an average of ~3.6 x 10^4 m^3 s^{-1} (Meade et al.,1983; Muller-Karger et al., 1989;Vörösmarty et al., 1998). Low discharge occurs during the dry season (January–May) and high discharge during the rainy season (July–October) as a result of the meridional migration of the ITCZ.

The fresh water discharges from the Amazon and Orinoco Rivers spread outward into the western equatorialAtlantic Ocean while continually mixing with surroundingsalty ocean surface water. The averaged geographicaldistribution of the low-salinity signatures of the Amazonand Orinoco River plumes can be revealed with historical in situ surface salinity data. However, only satellite remote sensing data is known to provide means to monitor the wide surface dispersal of these two fresh pools, with ocean color data being the first to illustrate Amazon plume reach to well beyond 1000 km (Muller Karger et al., 1988). Since these first observations, the application of ocean color, altimetry, and SST satellite mapping in this region has increased in its sophistication, showing the ability to track surface plume area (e.g. Hu et al., 2004; Molleri et al., 2010), fronts along the shelf to the North West (Baklouti et al., 2007), and northward propagating eddies or waves shed near the North Brazil Current (NBC) retroreflection region, the so-called NBC rings (Ffield, 2005; Goni and Johns, 2001; Garzoli et al., 2004).   In each case, the satellite data are able to provide time-resolved information on advective processes up to certain limits that include cloud cover, minor SST and ocean color gradients, non-conservative dilution processes for the ocean color to salinity conversions (Salisbury et al., 2011), and baroclinicity and subgrid variability of the altimetry Seas Surface Height Anomaly (SSHA) tracking of the NBC rings. As first evidenced by Reul et al., 2009, passive remote sensing data at low microwave frequencies can be successively used to complement these more 'classical' satellite observations to better follow the temporal evolution and spatial distribution of surface salinity within and adjacent to the Amazon River Plume.

To illustrate this new capability, we first show in Figure 2 comparisons between collocated SMOS SSS and *in situ* Conductivity-Temperature Depth (CTD) measurements acquired during the Geotraces West Atlantic cruise leg 2 across the Amazon river plume in June 2010. This campaign was conducted on RV Pelagia in the frame of the GEOTRACES international program (see http://www.geotraces.org/).

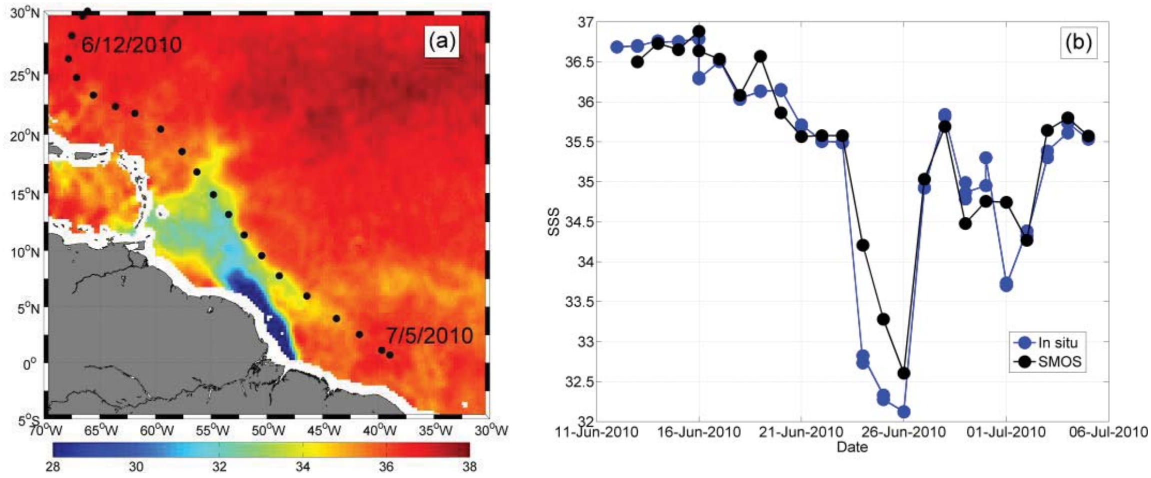

Figure 2: *(a) Black dots: location of the CTD stations conducted during the Geotraces West Atlantic cruise leg 2 (RV Pelagia) from 11 June to 5 July superimposed on the SMOS averaged SSS from June 12th to July 5th 2010. (b) Co-located surface salinity between SMOS and in situ data along the leg. SMOS data have been averaged at 50 km resolution with a ±5 days running temporal window.*

Comparison between satellite and 3-m depth *in situ* SSS data reveals an overall good agreement with a standard deviation of the difference SSS_{SMOS}-SSS_{CTD} of ~0.45. In particular, the strong gradient and ~3 unit drop observed as the R/V Pelagia leg crossed the Amazon river plume is well detected by the satellite observations.

New sea surface salinity products from satellite plateforms such as SMOS allow in particular to gain insights into the advection pathways of the fresh water Amazon and Orinoco river plume along surface currents. For the first time, SMOS sampling capability thus enables imaging the plume structure almost every 3 days with a spatial resolution of about 40 km. Combining SMOS SSS with altimeter-derived geostrophic currents and wind-driven (Ekman) estimated motions (Lagerloef et al., 1999), the advection of the spatial patterns of low salinity discharged from the major river mouths can now be analyzed systematically with an unprecedented resolution.

As illustrated by the Figure 3 and by the animation available at http://www.ifremer.fr/naiad/salinityremotesensing.ifremer.fr/altimetry_amazon_atl.gif, a very good visual consistency is found between the geostrophic and Ekman surface current pattern estimates and the SMOS SSS spatio-temporal distribution along the year.

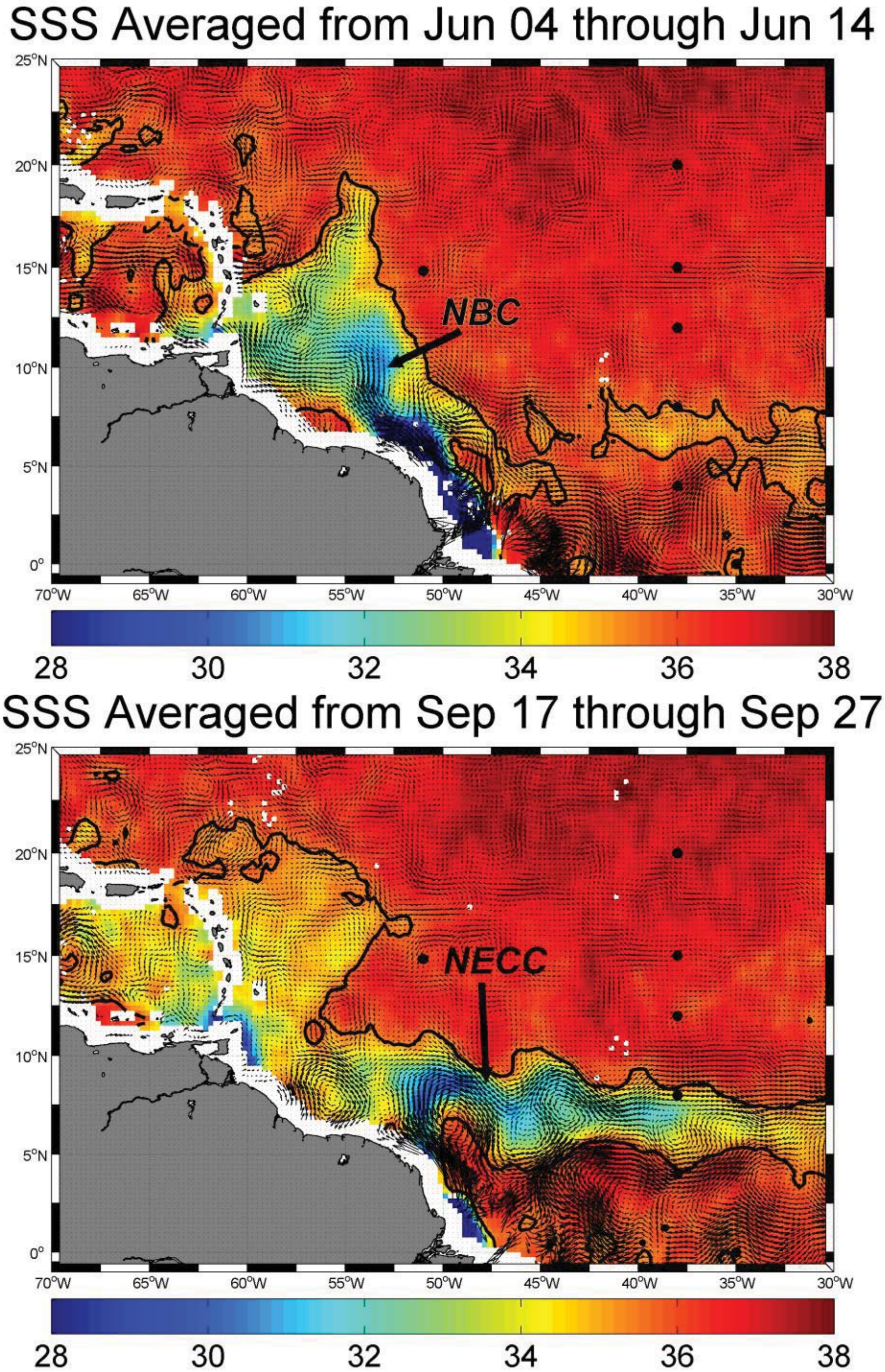

Figure.3 *Major pathways for the freshwater Amazon-Orinoco river plume detected by SMOS in 2010. Surface salinity fields from SMOS are superimposed with coinciding surface OSCAR currents estimatedfrom altimetry and surface wind data. Top: the freshwater Amazon river plume is advected northwestward along the Brazilian Shelf by the North Brazilian Current (NBC) during boreal spring. Bottom: during boreal summer to fall period, the Amazon plume is carried eastward by the North Equatorial Counter Current (NECC). Note also the signal from the Orinoco river plume extending Northeastward along the southern lesser Antilles. In both plots the thick black curve is indicating the 35 SSS contour.*

Mignot et al. (2007) show a long-term seasonal to monthly climatology that highlights two fresh water offshore pathways - the north passage to the warm pool and eastward entrainment into the North Equatorial Counter Current (NECC) – but they cannot clearly confirm or track this laterally with time in a given year.

SMOS SSS data combined with altimetry and surface wind information now enable to follow the spatio-temporal evolution of the plume along these twofresh water offshore pathways.

As illustrated in Figure 3 (top), the surface fresh water dispersal patterns of the Amazon river plume are closely connected to the surface current topology derived from the merged altimeter and wind field product. As also evidenced earlier from several hydrographic surveys (e.g., Hellweger and Gordon, 2002), it is clearly apparent in the satellite imagery that the NBC rings are key factors in modulating the fresh water pathways of the Amazon plume from the river mouth at the equator towards higher latitudes up to 20°-22°N.

Eastward entrainment of low salinity water from the mouth of the Amazon river into the North Equatorial Counter Current (NECC) is also evident in the SMOS data for the second half of the year 2010 (see Figure 3, bottom). During that period, fresh water dispersal structure exhibits a zonal wavy pattern centered around ~8°N induced by current instability waves shed near the North Brazil Current (NBC) retroflection region (52°W,8°N). To analyze the freshwater plume transport and the evolution of salinity along Lagrangian paths following such wavy patterns, hypothetical drifters were dropped around the mouth of the river at the beginning of June and temporally advected with the surface currents deduced from merged altimeter and wind products. The evolution of sea surface salinity from SMOS L-band and AMSR-E C-band sensors (see Reul et al., 2009 for details on the AMSR-E SSS product), sea surface temperature analysis products and merged MERIS-MODIS Colored Dissolved Organic Matter (CDOM) absorption coefficient was estimated by interpolating the data in space and time along the path of such drifters.

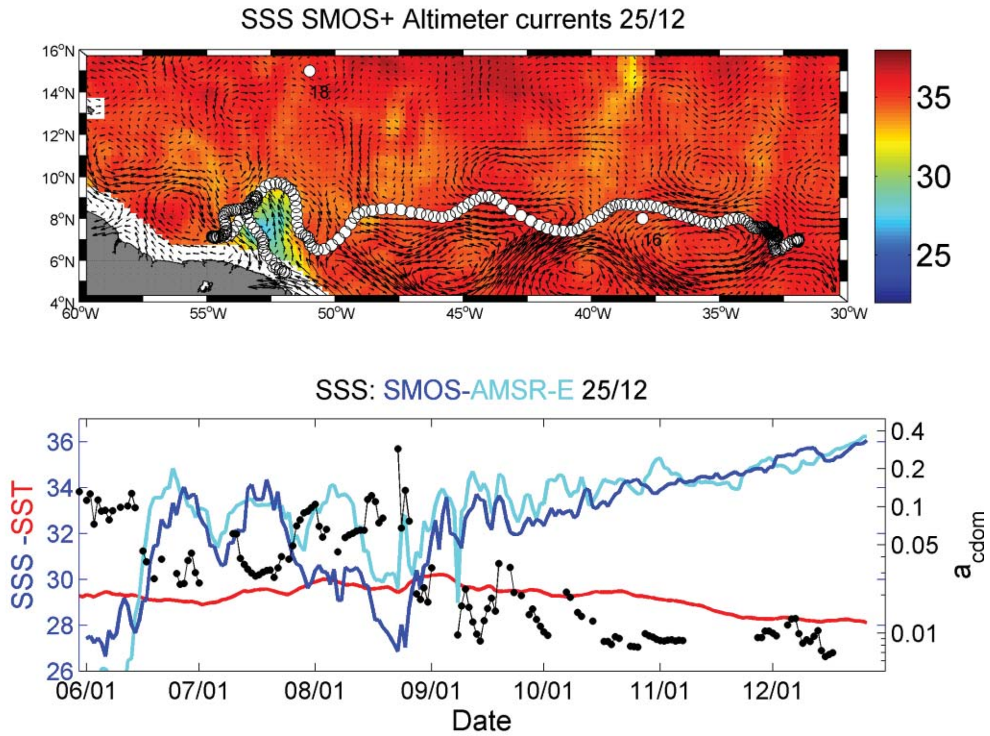

Figure 4: *Top:spatio-temporal evolution of the location of an hypothetical drifter (white dots) dropped at 52°W6°N at the beginning of june 2010 and advected with surface currents estimated from altimetry& surface winds (arrows). Superimposed are the +/-5 days averaged daily SSS fields from SMOS and the surface currents (black arrows). Bottom: time series of the co-localized SSS from SMOS (blue) and from AMSR-E (cyan), the analyzed SST (red), and the merged daily CDOM (black) along the drifter path.*

As further illustrated by the example shown in Figure 4, it takes approximately 6 months to cover a distance of 3700 km for a fresh water particle (SSS~26-28) in the proximity of the Amazon mouth to relax to an open ocean surface salinity of ~36. At the beginning of the period, the low SSS of water particles is modulated by mixing processes with saltier waters transported westward by the NBC rings shed at the NBC retroflection. The particle-following SSS signal modulation observed here is clearly consistent with the ocean color signal (anti-correlated to SSS), fresher water being systematically associated with colored waters showing high CDOM values, typical of the brackish plume waters. The drifter is then advected eastward along the NECC, remixed with 'younger' advected plume waters in August and reached an eastern position slightly north of 8°N-38°W with an SSS of about 32 at the beginning of October. The SSS change along the drifter pathway is progressively and quasi-linearly relaxing to the open ocean values during the next 3-month period.

The link between the SSS and ocean color properties moreover enables investigations of the interactions between bio-optical and bio-chemical properties of the ocean and hydrological fluxes of terrestrial origin. Along with the fresh water, the Amazon provides the largest riverine flux of suspended (1200 Mt y^{-1}) and dissolved matter (287 Mt y^{-1}), which includes a dissolved organic matter (DOM) flux of 139 Mt y^{-1} (Meybeck and Ragu 1997). These fluxes can have a dramatic effect on regional ecology as they represent potential subsidies of organic carbon, nutrients, and light attenuation into an otherwise oligotrophic environment (Muller-Karger et al., 1995).

In the most proximal regions of the Amazon Plume, light attenuation by suspended detritus acts as the main limitation to phytoplankton growth (Demaster and Smith, 1996). Away from this region, as mineral detritus is removed by sinking, absorption attributable to organic substances begins to dominate the attenuation of light in surface waters. DelVeccio and Subramaniam (2004) studied such conditions in the Amazon Plume and characterized the relative contributions of CDOM, particulate organic material and phytoplankton to the total absorption field. In the coastal ocean adjacent to river sources, CDOM tends to behave as a fresh water tracer, decreasing away from the river source with increasing salinity. Linear correlations between CDOM and salinity in river plume waters are well documented in ocean color literature with reported relationships robust enough to allow salinity retrievals from CDOM and vice versa (e.g. Ferrari and Dowell, 1998; Palacios et al., 2009; D'Sa et al., 2002; Conmy et al., 2004).

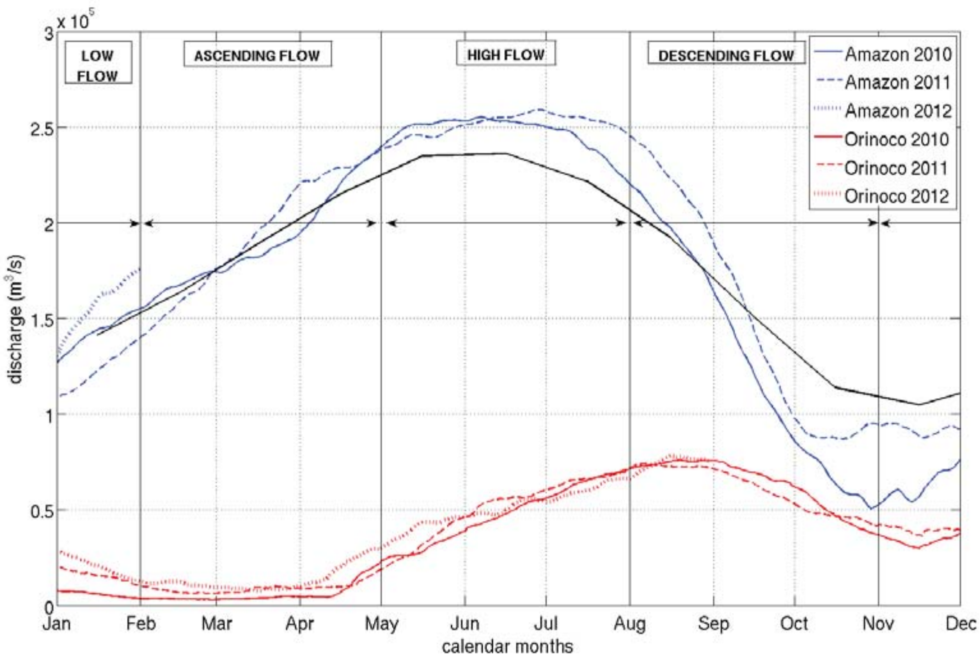

Figure 5:*Amazon (blue) and Orinoco (red) River discharge cycles measured respectively at Obidos and Bolivar gauges, during the period 2010- 2012. The black curve is showing the Amazon river discharge climatology from 1968 to 2012.*

Linearity in the CDOM – salinity relationship implies conservative mixing dominated by two distinct endmembers. Departures from linearity can occur when additional water masses are present (Blough and Delveccio, 2002), or by *in situ* subsidies of CDOM released via net phytoplankton growth (Yamashita and Tanoue, 2004; Twardoski and Donaghay, 2001), microbial utilization (e.g. Moran et al., 1999; Obernostererand Herndl, 2000), or photochemical oxidation (e.g. Miller and Zepp, 1995).

Based upon preliminary satellite microwave SSS data from AMSR-E sensor and ocean color products, Salisbury et al., (2011) recently demonstrated the spatial coherence between surface salinity and the absorption coefficient of CDOM at 443 nm in the Amazon and Orinoco river plume-influenced waters. Given the new SMOS data, the spatial and temporal coherence between SSS and optical properties of the river plumes, e.g. CDOM, can now be systematically analyzed.

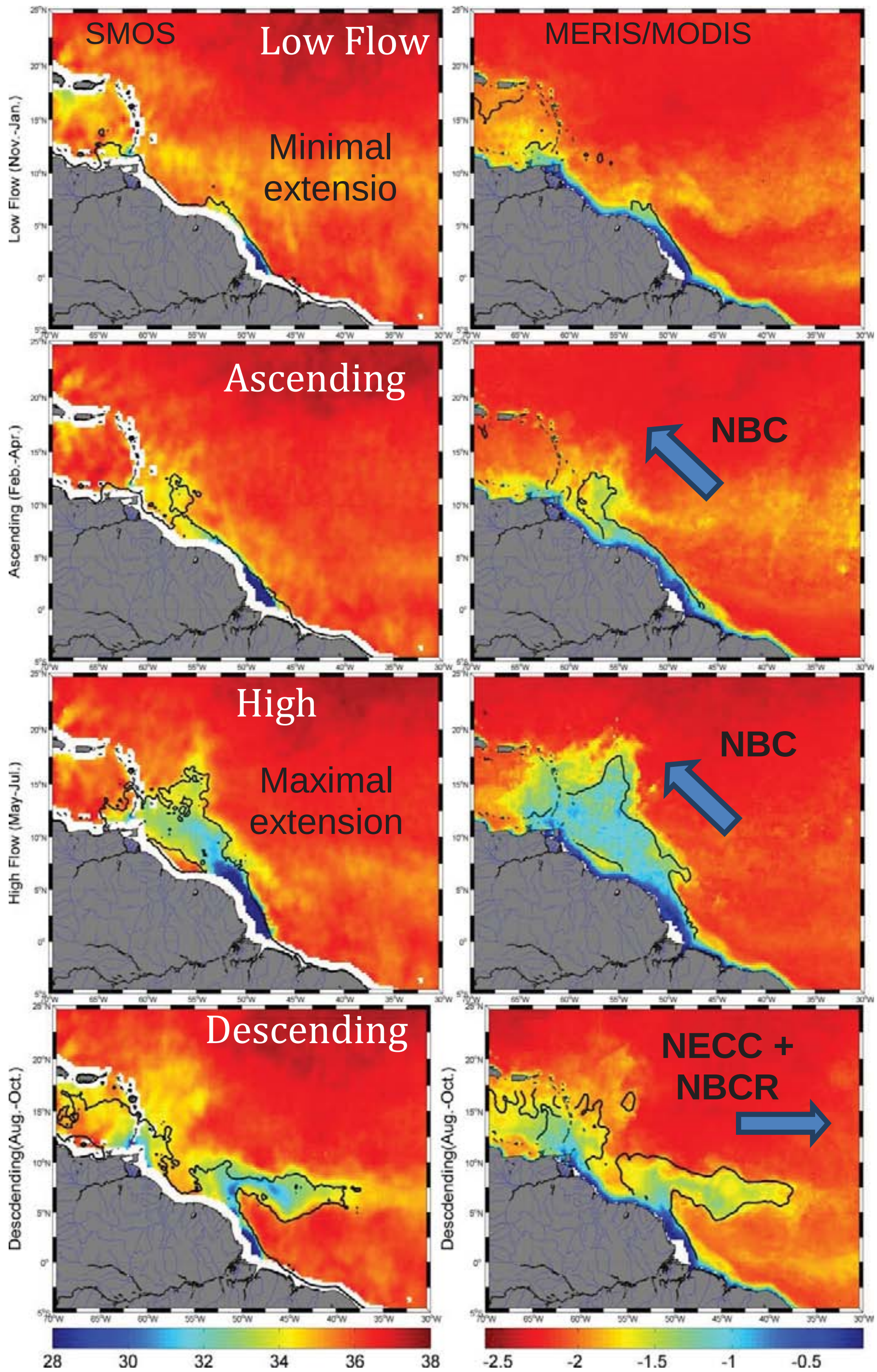

Figure 6: *Seasonal cycle of the freshwater Amazon and Orinoco river Plume signals for year 2010. Left: SSS from SMOS averaged over the different periods of the discharge cycle. From Top to bottom: Low Flow (Nov-Jan); Ascending flow (Feb-Apr); High-flow (May-Jul);Descending flow (Aug-Oct). Right: corresponding CDOM absorption coefficient averaged from the merged MERIS/MODIS products. The colorbar is logarithmic in unit of 1/m.*

As illustrated in Figure 5, the amplitude of the annual cycle of the Amazon river discharge peaks in June-July and was apparently more important in 2010 and 2011 compared to the averaged 'climatological' cycle since 1968. In comparison the discharge from Orinoco is much lower and peaks in September. Based upon the Amazon river discharge cycle, four main periods can be distinguished as shown in Figure 6. From November to April (low flow and ascending periods), the plume is carried northwestward with the NBC while the summer and fall display a plume mostly carried eastward as the seasonal NECC retroflection strengthens. In comparison, the spatial pattern in the distributions of the CDOM are in general very similar to SSS during the river discharge seasonal cycle. However, the CDOM patterns can deviate from the SSS patterns at large distances from the mouth of the river for some period of the seasonal cycle. This is particularly evident in the region around the northern Antilles and the Caribbean during the High flow season of 2010 (Figure 6, third panel from top) wherby high CDOM values are detected north of the low salinity plume extent (contours at SSS=35.5 on the right panels) suggesting presence of dissolved organic matter concentrations that are non-correlated with the Amazon river plume dilution. Altogether, this demonstrates the strength in combining satellite SSS observations with complementary satellite observations in order to better characterize the variability of the pathway of freshwater runoff along with the corresponding mixing processes at seasonal to interannual time scales.

Quasi-linear relationships between SMOS SSS and the MERIS/MODIS CDM absorption coefficient (acdm) estimated for year 2010 are illustrated in Figure 7. Acdm values were averaged over SSS bins with 0.5 pss bin width. As evidenced, while CDOM mixing processes seem to be conservative on average, clear departure from linearity are observed below 30 pss during the Descending and Low-flow seasons. This fact potentially indicates changes in the endmember values at the mouths of the rivers and tributaries and/or, illustrate occurrence of non-conservative mixing processes as listed above. Thanks to the new satellite observations, departure from conservative mixing and the inter-annual sources of variability will be certainly more detailed in the next future.

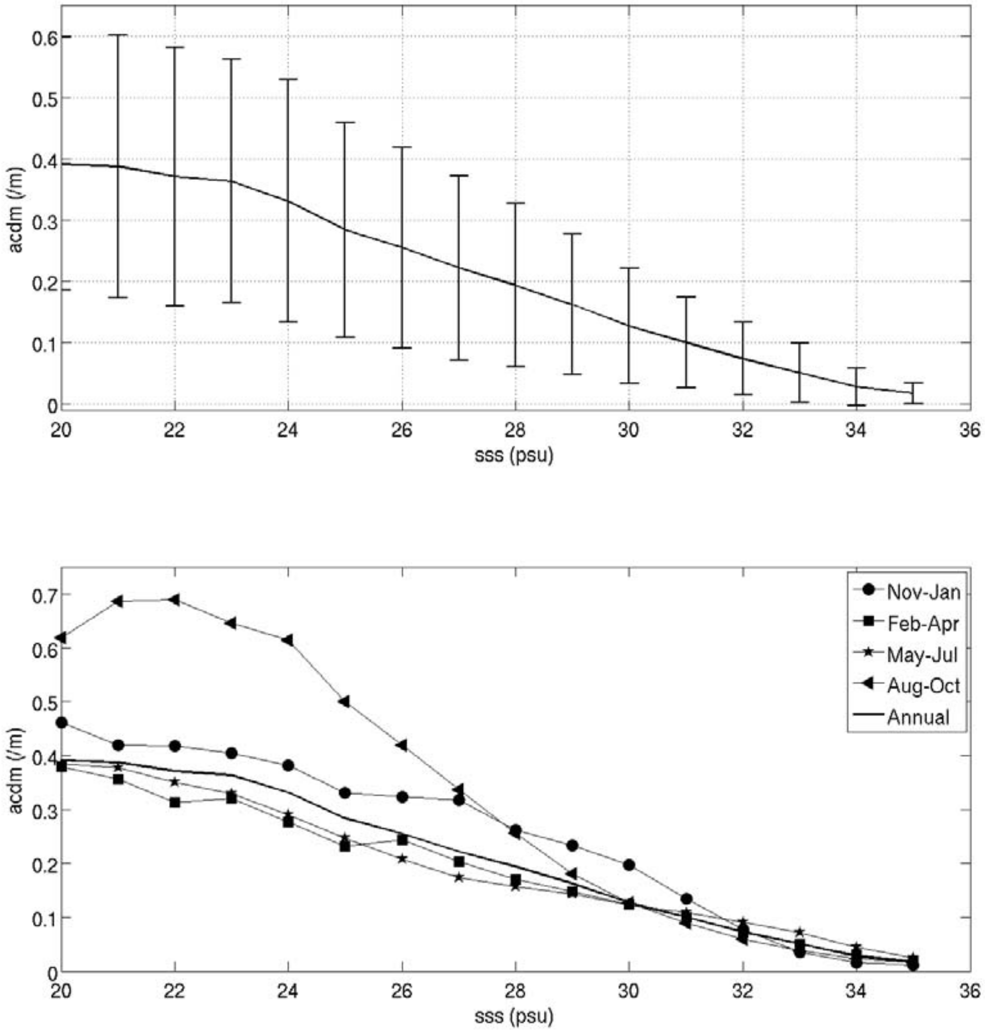

Figure 7: *$a_{CDOM}(490)$ to SMOS SSS dependence in the Western Tropical North Atlantic averaged over years 2010-2012 for all seasons of the Amazon River Discharge cycle (Top) and for each season separately (bottom). In the upper panel, the mean $a_{CDOM}(490)$ per 0.5 pss bins is shown as a solid black line ±1 standard deviation (vertical bars).*

3.2 Eastern Tropical Atlantic Freshwater Pools Monitoring

The Eastern Tropical Atlantic (ETA) Ocean 8°W-12°E,6°N-20°S is a region of intense upwelling and where the second largest river in the world, the Congo, enters the ocean together with the Niger, Volta and numerous other smaller rivers (Figure 8). In addition, intense precipitations also decrease SSS in the Guinea current and Northeastern Gulf of Guinea (Hisard, 1980; Merle, 1980). The ETA is therefore characterized with a highly complex hydrographic system, largely influenced by the Congo River, intense precipitation, and strong seasonal coastal and equatorial upwelling in the boreal summer.

Maximum discharge from the Congo River occurs in December and minimum discharge in March through April. The outflow is hardly detectable from SST or sea level data. In chlorophyll, however, the mouth of the Congo River shows a strong signal all year round with large plumes extending offshore. While these ocean colour signals highlight real oceanographic features of the plume, frequent cloud cover found in this region during the rainy season strongly inhibits the spatio-temporal evolution of the Congo plume structure to be monitored.

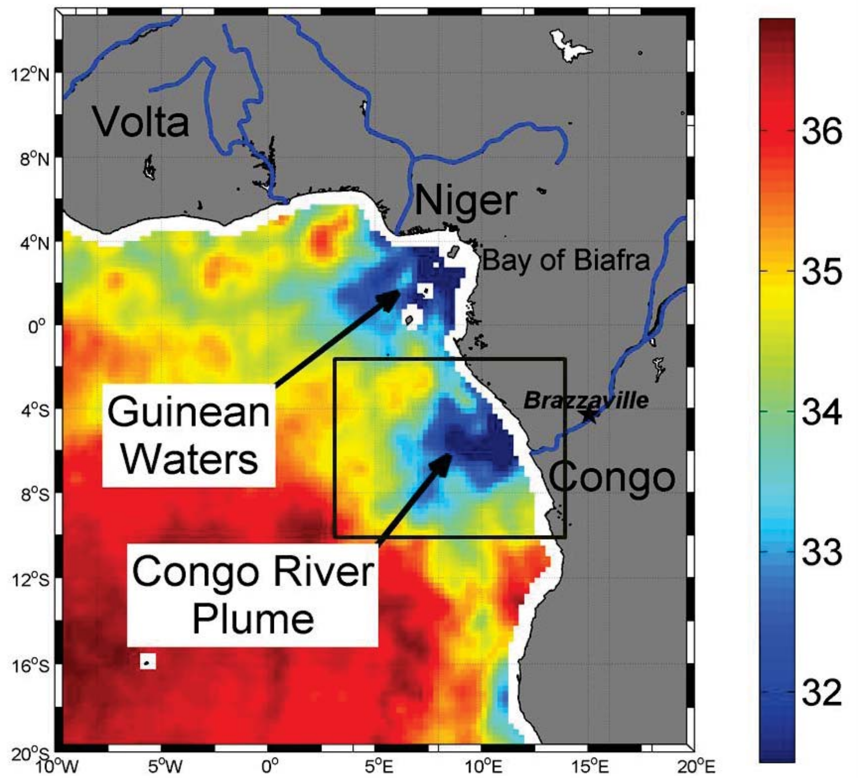

Figure 8: *Map of SMOS SSS in the Gulf of Guinea and Southeast Atlantic Ocean indicating the two largest pools of low salinity waters in the eastern tropical Atlantic: the Bight of Biafra (Guinean waters) and the Congo River plume. The map was generated by averaging SMOS data over 2010-2012 considering only data acquired during months of April.*

Hitherto the knowledge about the seasonal extension and spreading of the Congo river plume is therefore mainly relying on dedicated *in situ* surveys (e.g. see Meulenbergh 1968; Koleshnikov, 1973 ;Bornhold, 1973; Wauthy, 1977;van Bennekom et al., 1978; Eisma and Van Bennekom, 1978; van Bennekomand Berger, 1984; Piton andWacongne, 1985; Braga et al., 2004; Reverdin et al., 2007; Vangriesheim et al., 2009; Lefevre 2009). However, the ensemble of in situ SSS data collected during the period 1977–2002 in the ETA is sparse and only enabled retrievals of low-resolution (1°x1°) monthly climatology of the SSS field (Reverdin et al., 2007), as displayed in Figure 9. Since 2003 the *in situ* SSS sampling has improved with the increasing deployments and operations of Argo floats.

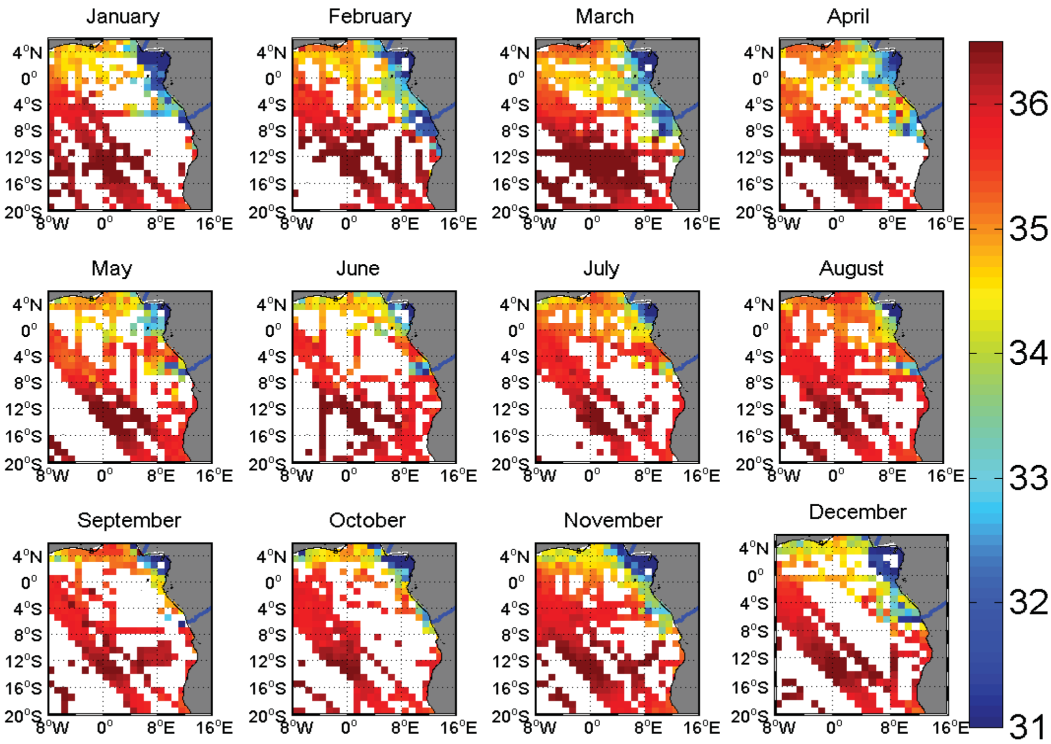

Figure 9: *Maps of the monthly averaged SSS in the ETA derived from the ensemble of in situ measurements collected during the period 1977-2002 and used to build up Reverdin et al. , 2007 climatology.*

The monthly averaged SMOS SSS maps shown in Figure 10 were generated by combining SSS data over the SMOS 3 years life period. As evidenced in detail by these maps, consistent with historical *in situ* observations, the Congo River plume is spreading north-westward along the coast and mix with southwestward flowing freshwater from the bight of Biafra during February and March (Koleshnikov, 1973 ; Wauthy, 1977). In May (Van Bennekom et al., 1978), June-July (Bornhold, 1973; Wauthy, 1977) and August (Koleshnikov, 1973) the two fresh pools are disconnected with the Congo plume directed in westerly direction, extending up to 800-1000 km offshore, as far as 8°E. In November, a "jet stream" of low salinity water is ejected from the estuary with a large velocity and protrudes in WNW direction (Wauthy, 1977). The plume extent can also show southward and south-westward legs depending on the prevailing windstress in the Angola Basin (Van Bennekom and Berger, 1984, Dessier and Donguy, 1994).

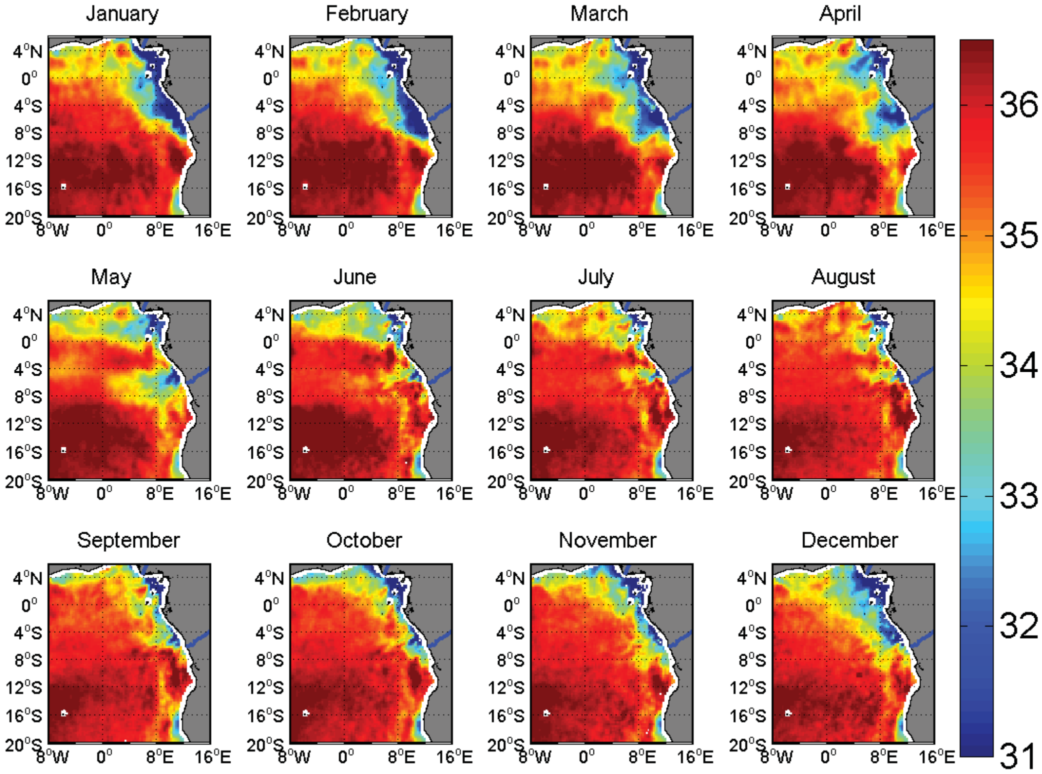

Figure 10: *2010-2012 monthly averaged seasonal cycle of surface salinity in the Eastern Tropical Atlantic derived from SMOS observations.*

The dispersal patterns of the Congo River plume during all seasons can mostly be included inside the rectangle domain shown in Figure 8. The 10-day running mean time series of the SMOS SSS averaged over that spatial domain is shown in Figure 11 together with the time series of the river discharge measured at Brazaville gauge station during the period 2010-2012. Maxima in the averaged SSS within that region occur regurarly in August at the time of the Congo river minimum discharge. Minima in SSS (detected around April) however lag by approximately 4 months the maxima in the river discharge at Brazaville station (found around December-January). These lags probably indicate the time for the freshwater masses to be transported from Brazaville to the river mouth and then to be further advected by surface currents far offshore. However, the inter-annual variability in the amplitude of the seasonal cycle of SSS and river discharge are not correlated. While the river discharge reached significantly different minimum values of ~3.3 x10^4m^3/s and ~2.3 x10^4m^3/s in 2010 and 2011, respectively, the maxima in the averaged SSS is constantly found at ~35.5 pss. Similarly, the maximum discharge level of ~5.8 x10^4m^3/s measured over the period is found in January 2012 while the minimum in the averaged SSS (~31.9) occurred in April 2011.

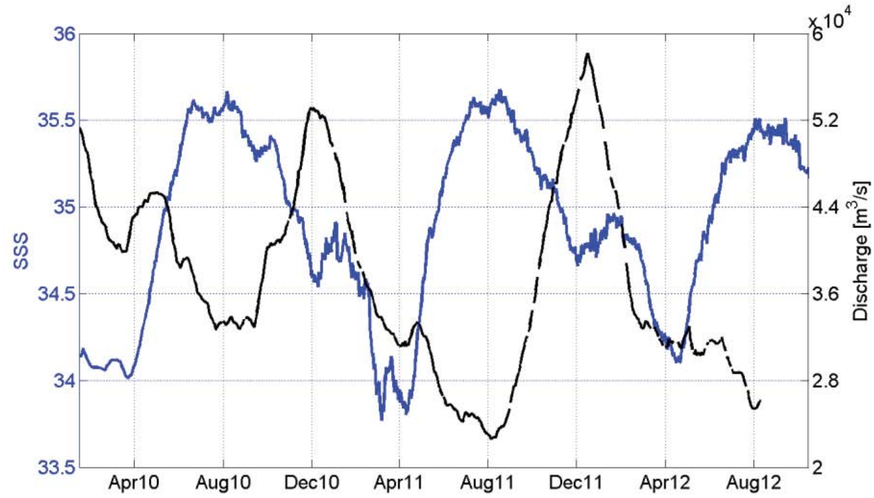

Figure 11: *Times series of (i) the SMOS SSS averaged over the spatial domain [3°E-14°E;10°S-2°S] illustrated by the black rectangle in Figure 8 (blue) and (ii) of the Congo discharge level measured at Brazaville (black).*

While understanding the observed satellite SSS trend in that region is still an undergoing activity, combining satellite information on surface currents, SST, rain rates and SSS together with River discharge levels will certainly help in the near future to better quantify the sources of variability in the local hydrological cycle of the Gulf of Guinea. The terrestrial and atmospheric hydrological fluxes in this region also act as a dominant modulator of the local fishery. The regular SMOS SSS data can therefore help to better understand the mechanisms involved in the biophysical interplay and its relevance for the fishery with potentially significant socio-economic impact in that region.

In addition, similarly to the Amazon-Orinoco river plumes, conservative mixing laws for bio-optical properties of the major river plume in the ETA region can now be systematically studied using SMOS data as shown in Figure 12. Examples of the conservative mixing linear laws for the CDOM coefficient deduced only from spaceborne measurements are shown for year 2010 around the Congo and Niger river.

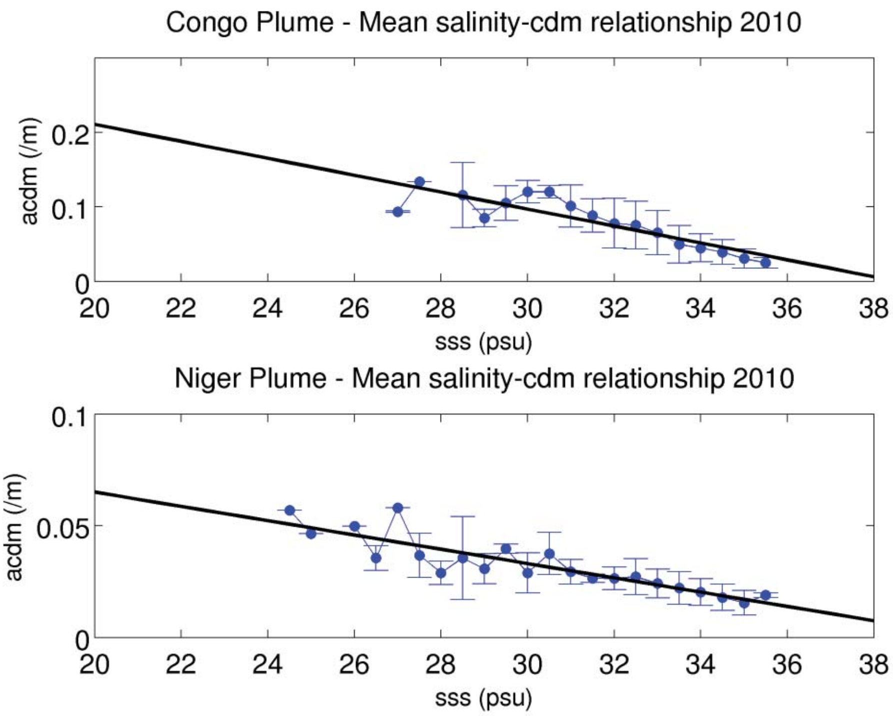

Figure 12: *a_{CDOM}(490) to SMOS SSS dependence in the Eastern Tropical Atlantic averaged over year 2010 for the Congo(Top) and Niger (Bottom) River Plumes. The mean a_{CDOM}(490) per 0.5pss bins is shown as a solid black line ±1 standard deviation (vertical bars).*

4. Precipitation signatures in SSS data from Space

Large vertical gradients can develop in the upper few meters of the ocean after a heavy rainfall, as first evidenced during the Tropical Oceans-Global Atmosphere Coupled Ocean-Atmosphere Response Experiment (TOGA COARE) (Soloviev and Lukas, 1996; Schlössel et al., 1997;Wijesekera et al. 1999). The downward fresh water flux at the sea surface establishes a haline diffusive molecular layer (or freshwater skin of the ocean) (Katsaros and Buettner, 1969) that is characterized by a salinity gradient, with salinity differences across this freshwater skin sometimes greater than 4 salinity unit. The residual effects of the rain-induced skin layers can even be stronger at the highest rain rates (Schlössel et al., 1997). This freshwater skin stabilizes the near-surface layer (Ostapoffetal., 1973) and tends to dampen free convection in the upper oceanic boundary layer.

These conditions motivate the development of autonomous sea surface salinity drifters able to monitor the salinity at less than 50 cm depth. Using such instruments, Reverdin et al., (2012) documented salinity freshening between 15 cm and 50 cm depth in the tropical

oceans. Sudden salinity decreases are often associated with local rainfall and vertical salinity gradients that last for a few hour, depending, among other factors, on wind speed conditions. The haline molecular diffusion layer that is established in the upper ocean during rainfall can thus be important for the radiometric observation of the sea-surface at low microwave frequencies. At centimeter wavelengths the dielectric constant is modified by the sea-surface salinity (e. g. Klein and Swift, 1977; Yueh et al., 2001) and any change of the latter might cause interpretation problems when comparing remotely measured surface salinity at these frequencies to deeper *in situ* measurements.
Hence, under rainy conditions (or just after a rainfall), satellite SSS shall better characterize the salinity at the ocean-atmosphere interface rather than the 1-10 m deep *in situ* samples. Whether accumulated precipitation can be estimated from changes in salinity at the ocean surface as observed from Space remains however an open question, as asumptions have to be made about the penetration depth of the fresh water. In addition, assimilation of the new satellite SSS data into ocean circulation models having limited vertical resolution also challenges our modeling perspectives concerning the dynamics of the first centimeters to first meter of the ocean surface.

In the following section, we discuss signatures of precipitation detected in the new SMOS SSS data. First, the strong SSS spatio-temporal variability associated with rain events as seen both by spaceborne and *in situ* sensors in the Pacific Ocean Inter-Tropical convergence zone is presented. Second, it is revealed that the SSS from space is systematically showing lower values (negative bias) with respect to the deeper 5-10 m depth of Argo upper salinity. These effects are shown to be statistically correlated with rain. Third, long-lived, large-area and large amplitude SMOS SSS anomaly patterns in the Tropical Atlantic are shown to follow local anomaly patterns in the Evaporation-Precipitation (E-P) budget. Finally, the preliminary results of the inter-annual variability of the SMOS SSS signal in the Indian and in the Tropical Pacific oceans and connections to key climate indexes will be presented and discussed.

4.1 SSS temporal variability associated with rain events

Although satellite observations provide a better sampling of the global ocean than the *in situ* observing systems, such as the Argo float array, individual SSS measurements are obtained in rainy regions with a strong temporal variability seen on both SMOS and Argo

SSS. In Figure 13, we show such an example of co-located SMOS and Argo profiler measurements in the InterTropical Convergence Zone of the Tropical Pacific indicating a significant surface freshening associated with a rain event. On 11 August 2010, the Argo float WMO id#4900325 detected a freshening of 0.9 between 20 m and 5.5 m depth (Figure. 13a). In contrast, the Argo profile derived on 22 August shows that the salinity between 30m and 5m depth is much more homogeneous with more saline water at 5m depth compared to the one recorded on 11 August.

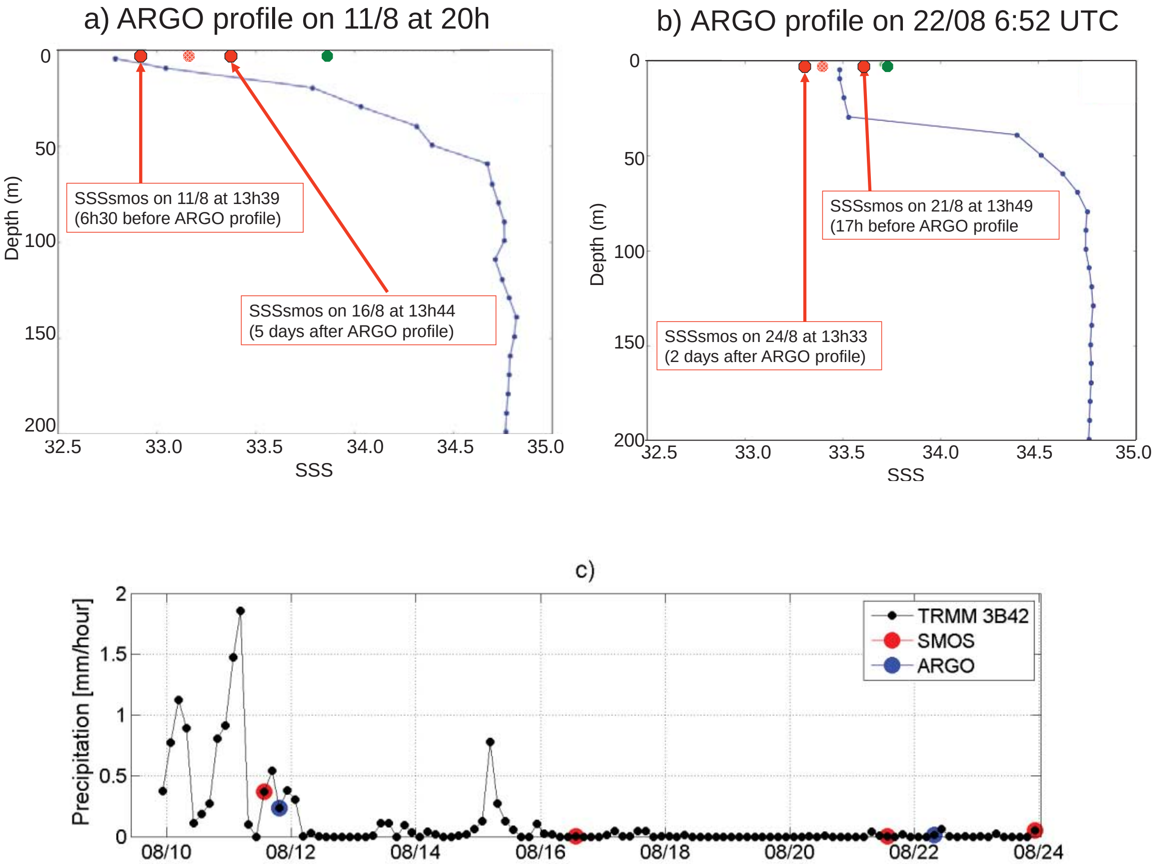

Figure 13:*Two successive Argo profiles taken by float 4900325 (blue curve) in the Eastern Tropical Pacific on (a) 11 August20:00 UTC (latitude=12.4°N; longitude=117.6°W) and (b) 22 August 6:52UTC (latitude:12.2° N; longitude: 117.8° W). Mean SMOS SSS collocated within a 5 days window and a radii of 50 km with these profiles are indicated by red dashed point. In each case, two SMOS passes have participatedto these collocations: mean SMOS SSS corresponding to each pass is indicated asred filled point. The corresponding ISAS SSS in August is indicated by the green point.The time series of the 3-hourly satellite rain rate from TRMM 3B42and averaged over [11°N-13°N; 116°W-118°W] is provided in c). The time at which SMOS and Argo acquired SSS data is indicated by red and blue dots, respectively.*

The TRMM satellite Rain-Rate (RR) estimates averaged over a 2°x2° box centered on the Argo float location indicate a significant rain rate of 1-2 mm h^{-1}on 11 August that lasted for at least a day before the Argo profile raised to the surface (Figure 13c). Contrarily, negligible precipitation occurred on 22 August and during the preceding week. The first SMOS pass collocated with the 11 August Argo profile (Figure 13a) was acquired also during rainy conditions and is showing a low SSS of ~32.8 (0.1saltier than the Argo SSS taken 6:30 h later, Figure 13c). The second SMOS pass on the 16th August occurred under non-rainy condition (Figure 13c) and is 0.5 saltier. Consistent with the 22 August Argo profile (Figure 13b) observations, the collocated SMOS SSS during these rain-free conditions (Figure13c) are also significantly saltier by 0.4-0.6. The large SSS variation (0.7) measured by this Argo float at a 10 day interval and by the collocated SMOS measurements over several SMOS passes clearly demonstrates the influence of the rain timing on the SMOS-Argo SSS differences.

4.2 Systematically fresher skin SSS in rainy regions

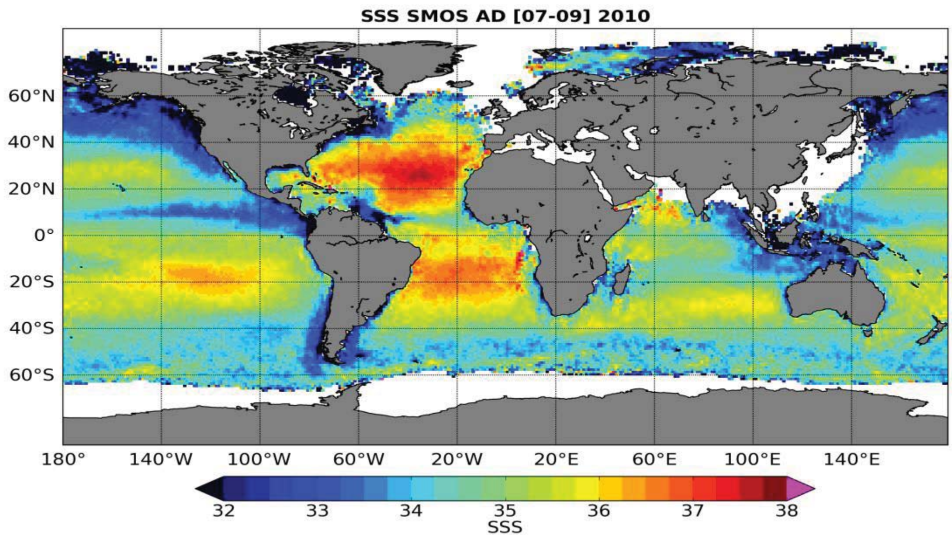

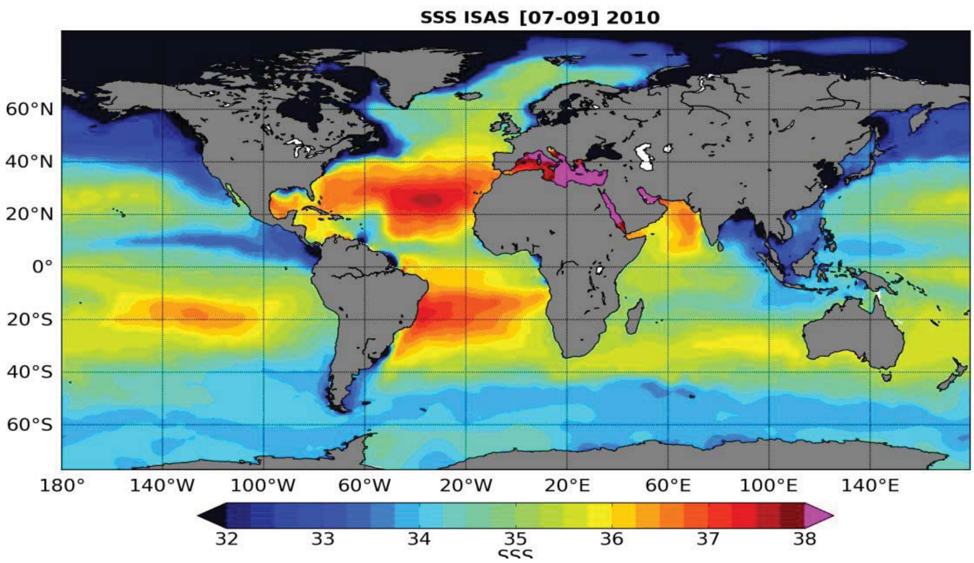

Figure 14: *Maps of SSS averaged from July to September 2010, derived from (top) SMOS ascending and descending orbits and ISAS (bottom).*

The SMOS SSS map averaged over July–September 2010 is compared to Optimally Interpolated *in situ* ISAS map averaged over the same period on Figure 14. At large scale, SSS spatial variability sensed by SMOS is consistent with ISAS. A striking visual feature of the SMOS SSS map compared to the *ISAS map* in the tropics is the freshest SSS in the North Tropical Pacific, under the location of the ITCZ (particularly west of 120°W).

	Mean (ΔSSS)	Std (ΔSSS)	*N*
Subtropical Atlantic Ocean (15°N–30°N; 45°W–30°W)	−0.13	0.28	206
Tropical Pacific Ocean (5°N–15°N; 180°W–110°W)	−0.23	0.35	692
Southern Indian Ocean (40°S–30°S; 70°E–90°E)	0.04	0.39	114
Southern Pacific Ocean (50°S–40°S; 180°W–100°W)	−0.08	0.51	467

Table 2.*Comparison of SMOS SSS (10day, 100×100 km2 average) collocated with Argo upper depth measurements.* $\Delta SSS=SSS_{smos}-SSS_{argo}$*Only SMOS ascending orbits are considered. Std (ΔSSS) primarily reflects the decreasing signal to noise* ratio *with decreasing SST. Note that subtropical Atlantic Ocean and tropical Pacific Ocean have similar SST.*

When SMOS SSS are precisely colocated around Argo SSS in various regions of the global ocean (see Boutin et al. (2012)), a more negative bias (~-0.1 than in other regions) and larger standard deviation are systematically observed between 5°N and 15°N in the Pacific Ocean with respect to other regions (Table 2).
To investigate if a systematic negative bias of ~0.1 between the satellite skin depth SSS and the ~5 m depth Argo floats data could be related to rain-induced vertical stratification, a triple collocation between Argo, SMOS Level 2 products (at ~40 km resolution, non averaged in time) and SSMI satellite rain rate (RR) data was conducted. SMOS and SSMI RR data were co-located within a temporal window of −40min and +80 min while a +/-5days windows was considered to co-locate SMOS and Argo data.

The theoretical error on the SMOS SSS retrieved Level 2 data used in this colocation exercise is ~ 0.5. Without any RR sorting, the statistical distribution of the differences *ΔSSS* is skewed towards negative values (Figure15 and Table 3); when only SMOS non rainy events are considered, the negative skewness disappears, and statistics of the SMOS-Argo differences in the Tropical Pacific Ocean become close to the ones in the subtropical Atlantic Ocean (Tables 2 and 3). Largest skewness towards negatives differences are obtained when only SMOS SSS close to rain events are considered. For these rainy SMOS cases, we find a negative dependency of the SMOS-Argo SSS differences with respect to SSMIs RR of −0.17pss/mm^{-1} h, i.e., a freshening of 1.7 for a SSM/I RR of 10mmh^{-1}(Boutin et al., 2012).

	Mean(ΔSSS)	Std(ΔSSS)	Skew(ΔSSS)	N
Tropical Pacific (5°N-15°N; 110°W; 180°W)				
All colocations	**-0.20**	**0.62**	**-0.38**	**38543**
No Rain (RR<0.1 mm hr^{-1})	**-0.13**	**0.56**	**0.01**	**29084**
Rainy (RR>= 0.1 mm hr^{-1})	**-0.40**	**0.73**	**-0.58**	**9459**

Table 3: *Statistics for the SSS differences $\Delta SSS=SSS_{smos}-SSS_{argo}$ as a function of Rain Rate (RR) in the Northern Tropical Pacific Ocean*

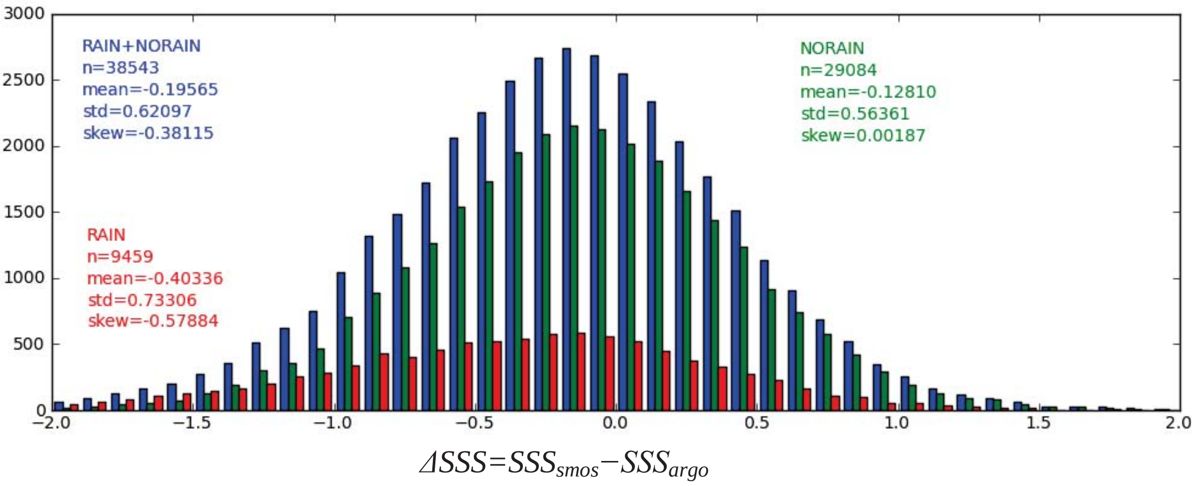

Figure 15: *Statistical distribution of SSS differences $\Delta SSS=SSS_{smos}-SSS_{argo}$ in the Tropical Pacific Oceanfor various sorting on co-located SSSM/I rain rates.Blue:all collocations (without any rain sorting); green: for non rainy cases (SSM/I rain rates less than 0.1 mmh^{-1}); red: rainy cases (SSM/I rain rates larger than 0.1 mmh^{-1}). Corresponding statistics are indicated in Table 3.*

The non sorting of SMOS measurements close in time with rain events in SMOS-Argo collocated datasets (within 10 days and 100 km) is responsible for (i) a mean −0.1 negative bias over 3 months between 5° N and 15°N in the Tropical Pacific region with respect to non rainy conditions and with respect to thesubtropical Atlantic region, and (ii) a negative skewness of the statistical distribution of SMOS minus Argo SSS difference (Figure 15). Given that the whole set of SMOS-Argo collocations also includes the situations with rainy Argo measurements collocated with non rainy SMOS measurements, these results indicate a systematic freshening of SMOS SSS in rainy conditions and is likely a signature of the vertical salinity stratificationbetween the first centimeter of the sea surface layer sampled by SMOS and the5m depth sampled by Argo. For more detail on the vertical SSS stratification induced by rain, the reader is also referred to Boutin et al. (2012b).

4.3 SSS as a tracer of the Evaporation-Precipitation budget in the oceanic mixed layer

The SMOS derived SSS can also be used to investigate the consistency between observed SSS variability and the Evaporation minus Precipitation budget in the ITCZ of the tropical Atlantic based upon the SSS and SST relationship in the ocean mixed layer (OML). The salt conservation budget in the OML with depth *h* can be expressed as follows (Michel, 2007; Yu 2010, 2011):

$$\frac{\partial S}{\partial t} = \frac{(E-P-R)S}{h} - \vec{u}\cdot\nabla S - \Gamma(w_e)\frac{w_e(S-S_h)}{h} + \kappa\nabla^2 S \quad (1)$$

where S is the surface salinity, E and P, the evaporation and precipitation rates, respectively, R the fresh water input by river runoffs, h, the mixed layer depth, $\vec{u}$ the (vertically averaged) current vector within the OML and w_e, the vertical entrainment rate. S_h is the salinity just below the OML, κ is the horizontal diffusivity coefficient (κ~2000 m.s^{-2}). The total entrainment term must be treated differently in case of upward or downward entrainment, so it is multiplied by a step function Γ in Eq (1). Indeed, when additional water is included into the mixed layer, its properties are affected by mixing with the deeper layer: $\Gamma(w_e)$=*we* if *we*>0. On the contrary, if water is removed from the mixed layer, the properties of the remaining water are conserved and only its depth *h* can change: $\Gamma(w_e)$=0 if *we*<0. The vertical processes are conveniently represented by a single entrainment term, consisting of the vertical Ekman advection and the OML conditions.

The first term in the right-hand side of Eq. (1) is the net fresh water flux. The impact of this flux on the surface water strongly depends on the salinity itself. Moreover, SSS has no direct feedback on the surface flux. These particularities have important consequences on the salt budget and on the duration of SSS anomalies. The second term is the horizontal advection of salinity by surface currents that can be separated into a wind induced component, the Ekman transport, and the geostrophic current. Ekman transport is due to wind friction on the sea surface, which is rotated by the Coriolis force as it penetrates in depth. The Ekman layer depth is systematically lower than the mixed layer depth, because both increases with the wind stress, although the depth of the mixed layer also deepens in response to other processes. Thus, the Ekman transport occurs entirely in the OML. In addition, the geostrophic current that arise from the balance between the horizontal pressure force and the Coriolis force can usually be considered constant the mixed layer resulting from the homogeneous density structure.

The value of the SMOS SSS at a fixed point***, S(t,r),*** is obtained by averaging individual SMOS swath SSS measurements over a considerable time interval (t-τ/2, t+τ/2), say 10 days, which is enough to filter out noise in the SSS. Suppose that the climate mean, or norm, of this SSS (provided by climatology) is $\overline{S(t,r)} = S_o(t,r)$. In the following, we define the SSS anomaly as the departure of the SSS from the norm:

$$\Delta S(t,r) = S(t,r) - S_o(t,r)$$

Following approaches traditionally used for studying large-area SST anomalies (Piterbarg, and Ostrovskii, 1997), a formal definition can be introduced for the large-area SSS anomalies. For example, large area and large amplitude SSS anomaly comprises the connected components of the set:

$$\{(x,y): |\Delta S(t,r)| > S_T\}$$

where r=(x,y) and S_T is a threshold that can be taken either as a fixed salinity value, for example, 0.2 pss, or as a function of the standard deviation of SSS anomalies, σ_S, for example 0.5 σ_S. This choice for the threshold depends on the magnitude of the anomaly of interest.

In the tropical Atlantic, Michel et al. (2007) and Yu (2011) have shown that the dominant terms of the mixed-layer salinity balance are horizontal advection by Ekman and geostrophic currents and the atmospheric forcing fluxes (E-P-R). In that context, the salinity balance equation in the OML can be simplified as follows:

$$\frac{\partial S}{\partial t} \cong \frac{(E-P-R)S}{h} - \vec{u}\cdot\nabla S \qquad \text{(Eq. 2)}$$

Using OSCAR surface current products (which comprise contributions of both Ekman and geostrophic currents), the horizontal salt advection term $\vec{u}\cdot\nabla S$ can be deduced from SMOS observations. The following residual SSS anomaly can then be estimated from SMOS temporal observations of salinity $S(t,r)$ at point r following:

$$\Delta S(t,r) = S(t,r) - S_o(t,r) - \vec{u}(t,r)\cdot\nabla S(t,r) \qquad \text{(Eq. 3)}$$

According to the simplified salinity balance (Eq. 2), *a priori* valid for the tropical Atlantic, the resulting SSS anomaly given by Eq.3 shall be strongly correlated with the net fresh-water flux forcing term. Examples for such SSS anomaly analysis is shown in Figure 16 for a selected point in the middle of the North Tropical Atlantic (16°N-35°W). From TRMM precipitation and OAFLUX daily evaporation fluxes, large-area P and E anomalies were also evaluated:

$$\Delta P(t,r) = P(t,r) - P_o(t,r)$$

$$\Delta E(t,r) = E(t,r) - E_o(t,r)$$

where P_o and E_o are the local climate mean for the precipitation and evaporation.

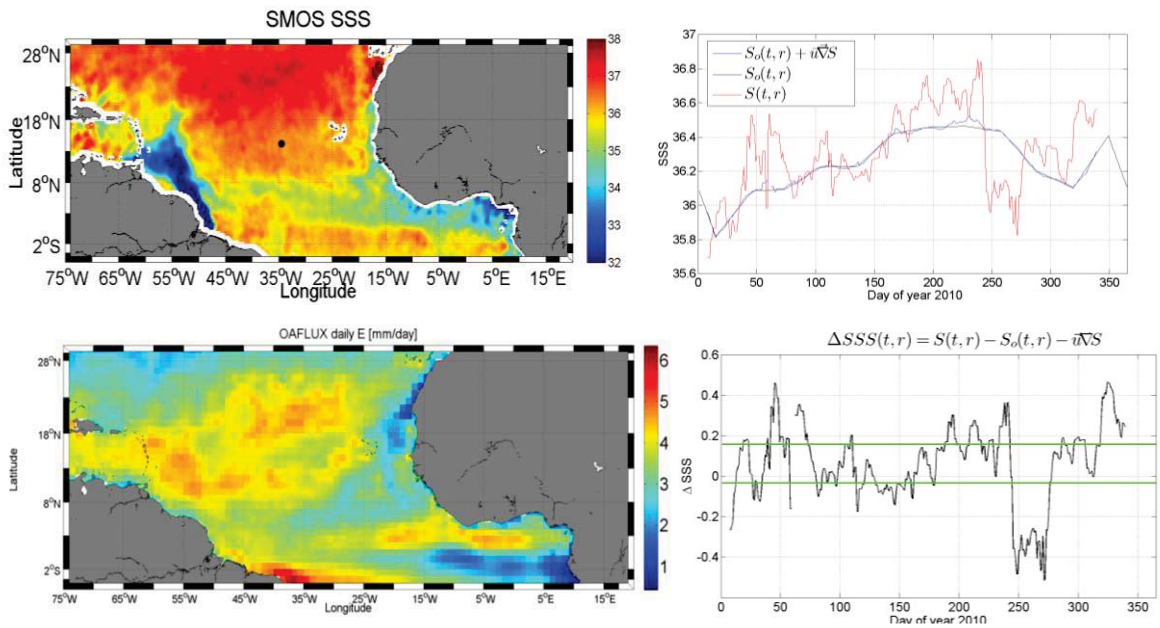

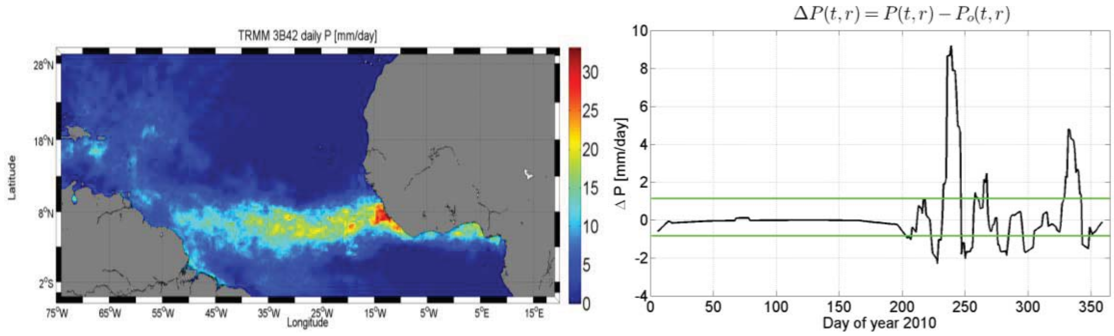

Figure 16: *Top left: SMOS 10-days SSS field in June 2010. Top right: time series of the surface salinity S(t) at the black point shown in the top left figure (35°W;16°N). Red: SMOS SSS, blue curve: local mean climatological annual cycle at that point $S_o(t)$. The resulting time series for the SMOS anomaly ΔSSS at that point is shown in the middle panel, right plot. The green horizontal lines are indicating ± one standard deviation of the local SSS anomalies, σ_S. In the middle and bottom left panels, we show the corresponding OAFlux Evaporation and TRMM 3B42 precipitation field (mm/day). The time series of the Precipitation anomaly at the point is shown in the bottom right panel.*

As illustrated in Figure 16 (middle right pannel), very significant long-lived negative ΔS(t,r) values are detected in SMOS anomalies at the selected point in the North Tropical Atlantic during September/October months (days 250-300) of 2010. Apparently, this happened just after a strong positive anomaly in the precipitation rate as detected from TRMM during the passage of the ITCZ in August (bottom right panel).

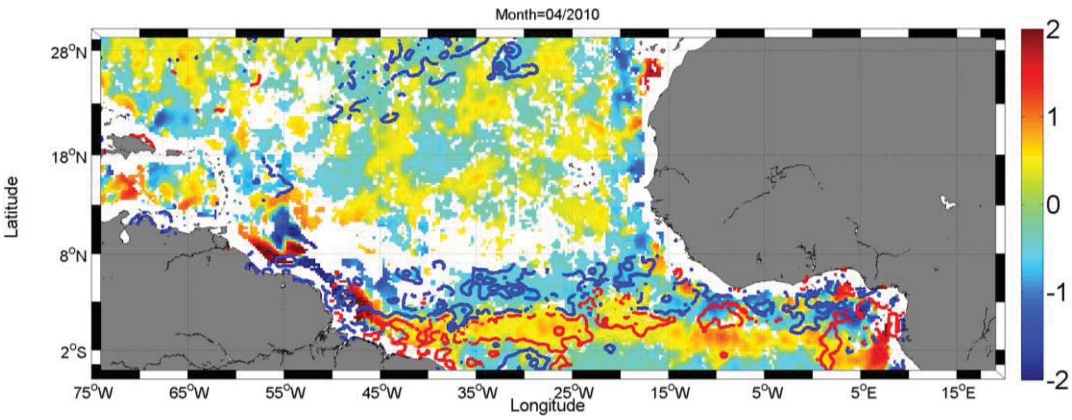

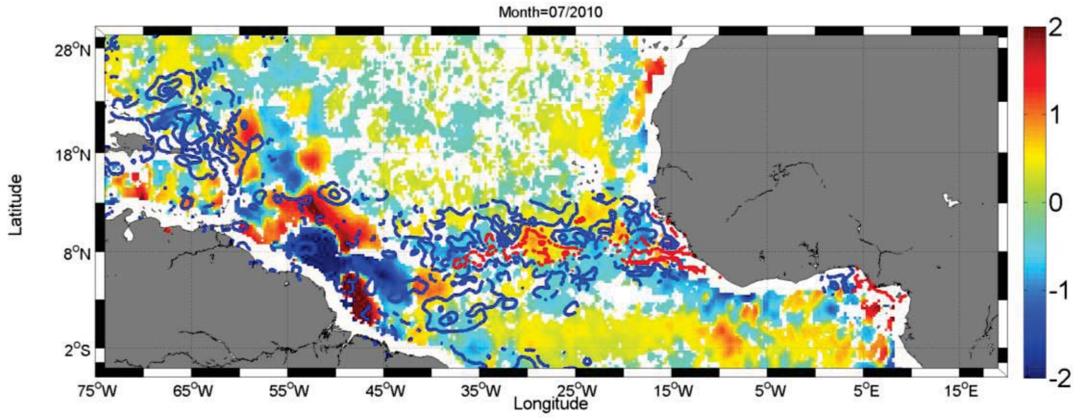

Figure 17: *Maps of the monthly averaged large amplitude SSS anomalies deduced from SMOS data for two selected months of 2010 (Top: month of march 2010;. Bottom: month of July 2010). The threshold value S_T used to derive the anomaly is defined by 1 σ_S, the local standard deviation of SMOS anomaly. Superimposed are the contours of the large positive amplitude Precipitation anomalies (blue) and positive Evaporation anomalies (red).*

The spatio-temporal consistency between the large area and large amplitude S, P and E anomalies can be further analyzed over all the Tropical Atlantic. This is illustrated in Figure 17 for two selected months of 2010. The spatial distribution of the large-area and long-lived (monthly averaged) SSS anomalies generally matches well the spatial patterns for the large E-P anomalies. In particular, North-South oscillation in ΔS(t,r) around the ITCZ (centered around 5°N in March and 8°N in July) follows the ΔE-ΔP(t,r) far from the Amazon plume area, with negative ΔS(r,t) corresponding to positive ΔP(t,r) and positive ΔS(r,t) found in region of positive ΔE(t,r). The average relationship between SMOS SSS anomalies and the corresponding anomalies in the net atmospheric fresh water flux in the tropical Atlantic (defined here by 5°S-20°N;75°W-15°E) was further evaluated over year 2010 by binning ΔS(t,r) values as function of ΔE-ΔP(t,r) as shown in Figure 18.

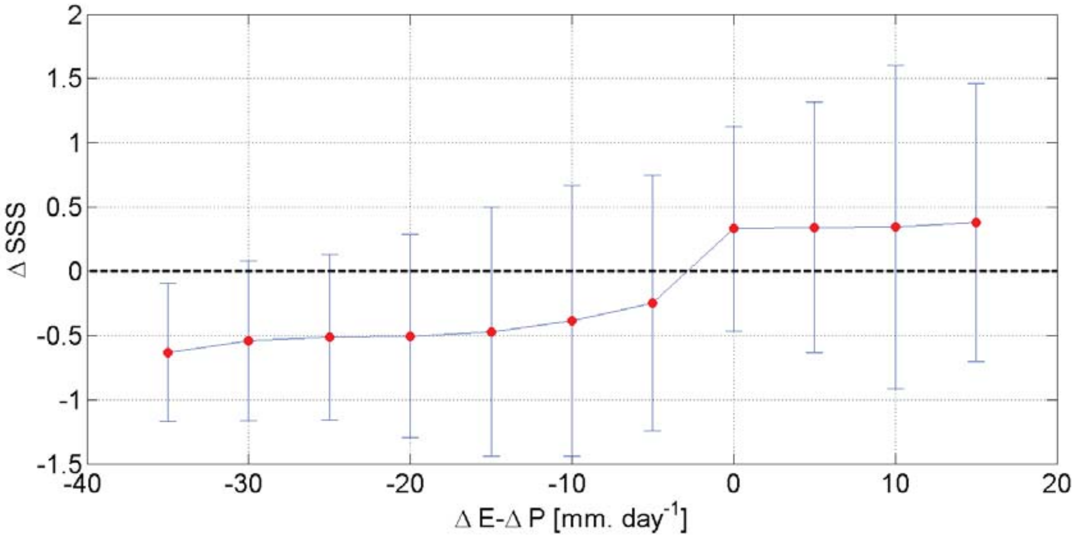

Figure 18: *Average relationship between SMOS SSS anomalies and the net atmospheric fresh water flux anomalies ΔE-ΔP in the tropical Atlantic (defined here by 5°S-20°N;75°W-15°E) over year 2010.*

Despite a significant scatter in the data, the results clearly indicate the strong coherency between SMOS SSS anomalies and the Evaporation minus Precipitation flux signal in the tropical Atlantic. On average, SMOS SSS are thus systematically fresher than the SSS climatology when Precipitation rate exceed Evaporation rate with respect climatological means, and vice-versa. As expected by the skin layer effects (Zhang et al. 2012), satellite SSS anomalies are weakly sensitive to excess evaporation showing an almost constant value whatever positive values for ΔE-ΔP. Nevertheless, and as discussed in section 4, the average 0.3 salinity unit excess amplitude found for ΔS in evaporative zones is significantly larger than the expected evaporation-induced effect on the satellite SSS (~0.01). The source for such observed signal amplitude is not yet understood. Other physical processes, not yet well accounted for in the SSS retrieval algorithm may systematically affect the L-band brightness temperature in strongly evaporative zone (e.g. skin effects in SST, badly accounted for roughness effects at low winds).

Nevertheless, Figure 18 clearly evidences that SSS anomalies become increasingly negative as the precipitation anomalies progressively exceed the Evaporation anomalies.

This shows that it is important to monitor SSS from Space in the rainy regions as it makes a good oceanic rain gauge for the changing water cycle [Cravatte et al., 2009; Yu, 2011, Terray et al., 2011], and therefore help tomaintain a continuous observation network in these key regions of the marine branch of the global hydrological cycle. In that context, SMOS SSS may therefore be an interesting dataset for assimilation into ocean models in the perspective of better constraining oceanic precipitation forcing terms.

4.4 Large scale SSS inter-annual variability in tropical Indian and Pacific Oceans

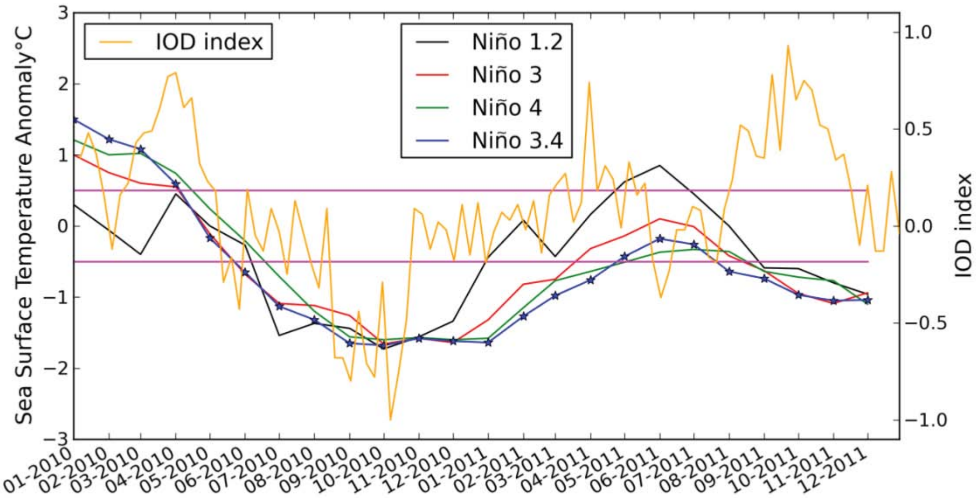

Figure 19:*Time series of SST anomalies in the four Niño regions from http://www.cpc.ncep.noaa.gov/data/indices/sstoi.indices in 2010-2011 and corresponding Indian Ocean Dipole (IOD) Index (SST difference between eastern and western equatorial Indian Ocean) from the Australian bureau of Meteorology (BOM).*

In the Indian and Pacific Oceans the precipitation impact on the large scale SSS variability can also be observedfrom SMOS and ISAS monthly maps.

The 2010-2011 period was characterized by a strong La Niña event lasting from July 2010 to March 2011 and by an Indian Ocean Dipole (IOD) index in negative phase in September-November 2010 and in positive phase during about the same months in 2011 (see Figure 19). Such events are known to generate large scale SSS signatures in the tropics (e.g.,Gouriou et al., 2002; Singh et al. 2011, Grunseich et al. 2011) and are clearly depicted in the SSS signals in both theISAS and the SMOS monthly difference maps between 2010 and 2011 for both July and November (Figure 20).

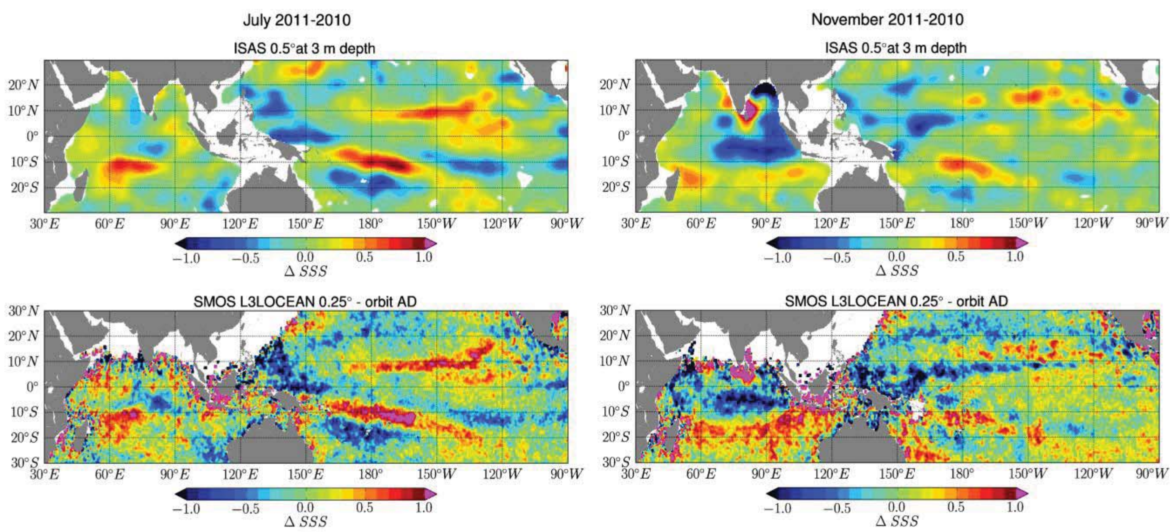

Figure 20 :*Differences in the monthly averagedSSS between year 2011 and 2010for months of July (left) and November (right). Top panels show the*$\Delta SSS=SSS_{2011}-SSS_{2010}$ *results obtained from in situ OI analysis products ISAS and bottomones from SMOS data.*

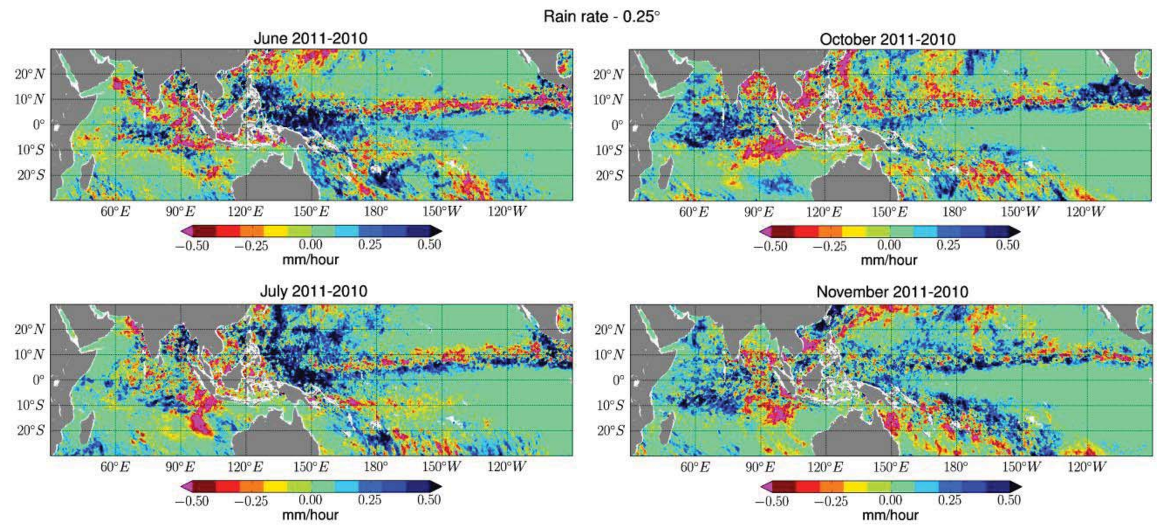

Figure 21:*Rain Rate differences* $\Delta RR=RR_{2011}-RR_{2010}$*derived from SSM/I F17 between 2011 and 2010 for months of June (Top left);July (Bottom Left); October (Top right) and November (Bottom right).*

The differences in rain rate as derived from SSM/I F17 sensor between 2011 and 2010 for several selected months as shown in Figure 21 further demonstrate that part of the observed SSS interannual variability for July and November are associated with large precipitations anomalies during previous months, associated with displacements of the ITCZ and of the South Pacific Convergence Zone (SPCZ). In the Indian Ocean, SSS differences $\Delta SSS=SSS_{2011}-SSS_{2010}$ observed in November indicate saltier SSS in 2010 than in 2011 in the eastern equatorial Indian Ocean within the band [10°S-0°;70°E-95°E] associated with a smaller rain rate ($RR_{2010}<RR_{2011}$) in the surrounding region during

preceding months, as evidenced by the rain rate difference on the October and November maps shown in Figure 21. Between ~10°S and 20°S, SSS are fresher in 2010 than in 2011; this is associated with higher precipitation in 2010 than in 2011(RR_{2011}<RR_{2010}) in the eastern basin but not over the whole basin. Patterns of positive SSS anomalies in the eastern equatorial Indian Ocean, and negative anomalies in the eastern part of the region south of ~10°S are quite consistent with SSS anomalies already reported during negative IOD coupled with a strong La Niña event (see Figure 8 of Grunseich et al. 2011).

Although patterns of 2011-2010 SSS differences are similar on SMOS and ISAS monthly maps, the differences are often more contrasted in the SMOS data (e.g., Figure 20, left part and Figure 22).

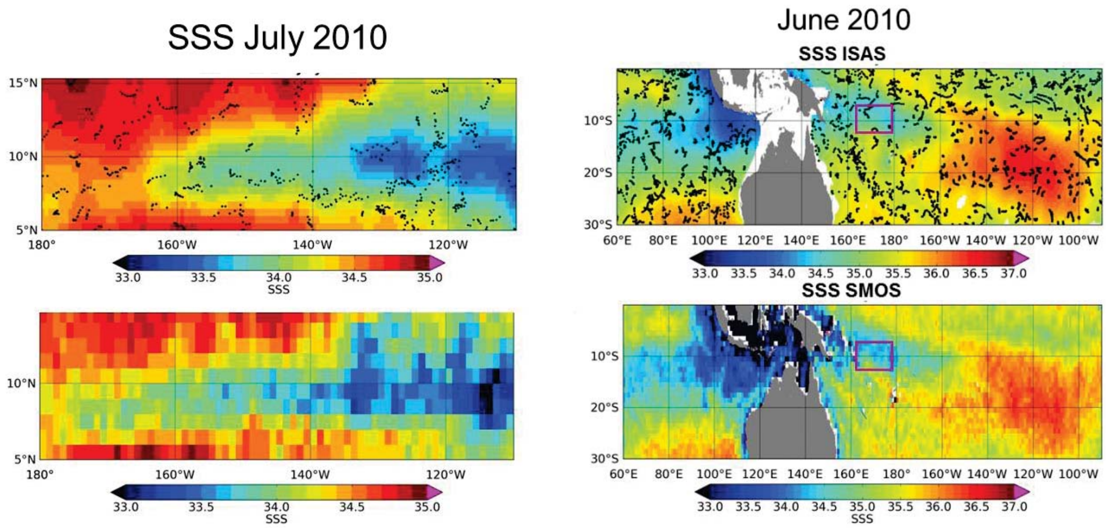

Figure 22: *Left: July 2010 SSS maps in the Northern Tropical Pacific Ocean from ISAS (top) and SMOS (bottom). Right: June 2010 SSS maps in south Pacific-Indian tropics from ISAS (top) and SMOS (bottom). In both top panels, the small black dots represent the locations of the in situ data samples used in the objective analysis. The purple square on the right figure indicates the region where the drifter discusses in Figure 23 evolved.*

This originates from fresher SSS seen in the SMOS SSS maps than in the ISAS SSS maps (Figure 22). In addition the spatial extent of the low SSS region appears wider in the SMOS map, as illustrated in Figure 22 left around 8°N. This is possibly due to the in situ measurements undersampling and/or smoothing by the OI applied to the ISAS. In addition, the SMOS freshening could be linked to the different depth of the measurements (SMOS at 1cm, and *in situ* SSS measured at several meters depths) as described in sections 4.1 and 4.2.

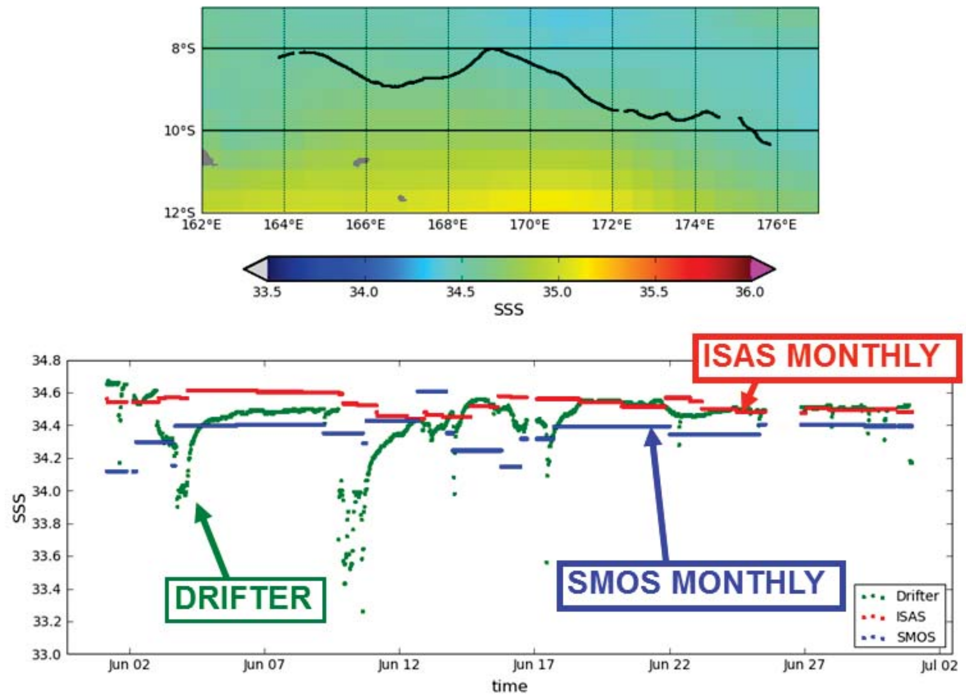

Figure 23:*Top: trajectory of a Surface Velocity Program (SVP) float in the western Pacific region measuring conductivity and temperature at 45cm depth. Bottom: SSS along the drifter trajectory measured by the drifter (green), derived from SMOS monthly map (blue), from ISAS monthly map (red).*

Finally, to illustrate the potential impact of thevertical stratification effect on the ΔSSS differences between satellite and *in situ*, we compare along the drifter trajectory the salinity measured at 45cm depth by a surface float (Reverdin et al. 2012) in the 2010 rainy western Pacific with monthly SSS maps (Figure 23). The drifter SSS data clearly indicates a large signature of rainy events, with typical freshening events larger than -1 and lasting for more than one day. The ISAS SSS is on the upper range of the drifter SSSwhile monthly SMOS SSS is systematically on the lower range in this rainy region. While more work is certainly needed to determine the physical sources for these observed differences, the vertical SSS stratification associated with rain events,as illustrated by this case, is a likely contributor to the different signatures in the inter-annual SSS variability as detected by the SMOS satellite SSS data and the Argo data.

These preliminary results confirms the capability of L-band radiometry in detecting large SSS signals and their low-frequency variability (here over a two-years period), in spite of much noisier satellite than in situ measurements. In general this results from much better satellite based spatio-temporal coverage and with a better spatial resolution, thus, offering complementary information to existing *in situ* measurements.

5. Fresh Pools interactions with wind-driven processes

In this section, two specific SMOS observation cases study cases of wind-driven phenomena are presented. The first example illustrates the erosion of the Far Eastern Pacific Fresh Pool by the gap-wind driven Panama Upwelling processes whereas the second focuses on the salty wake left behind hurricanes after their passing over the Amazon-Orinoco river plumes.

5.1 An example of Fresh Pool Erosion by wind-driven upwelling

The eastern tropical Pacific Ocean between about 120°W and South America is unique in many respects. Lying in an environment predominantly influenced by the South and North-Eastern trades and the doldrums, and seasonally affected by the winds from the Caribbean, this region is characterized by complicated and large seasonal variations in the wind field, current pattern, and temperature and salinity structure.

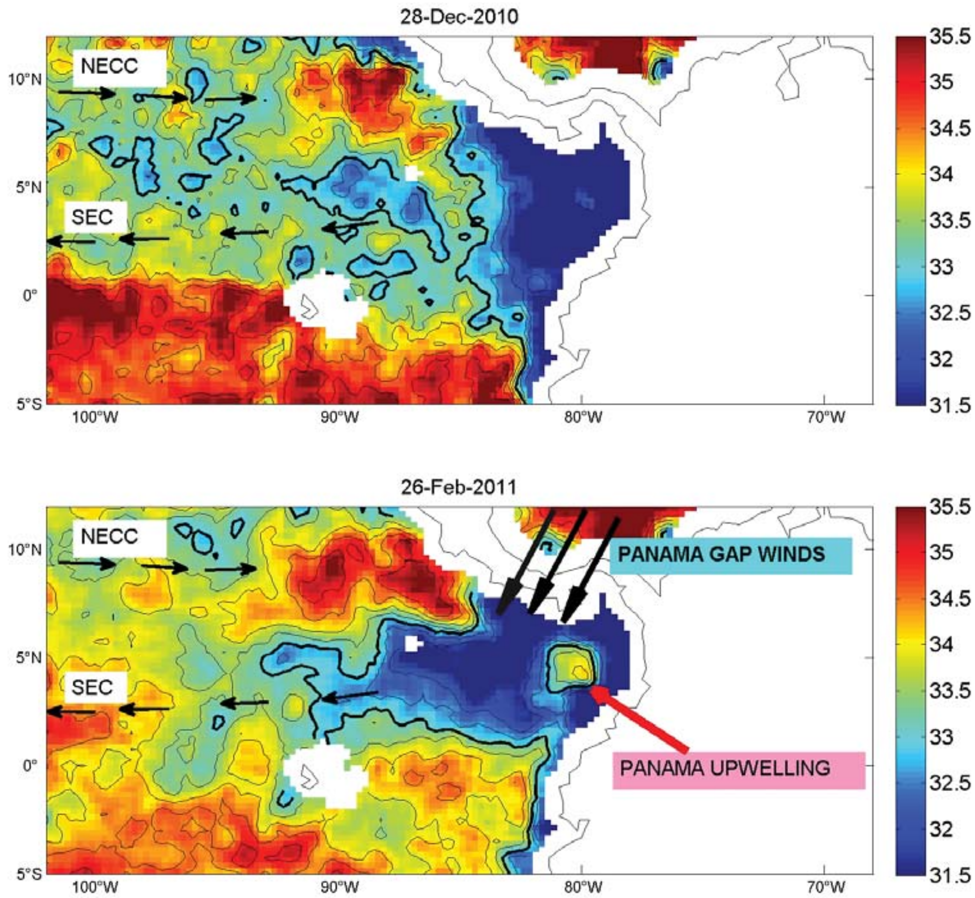

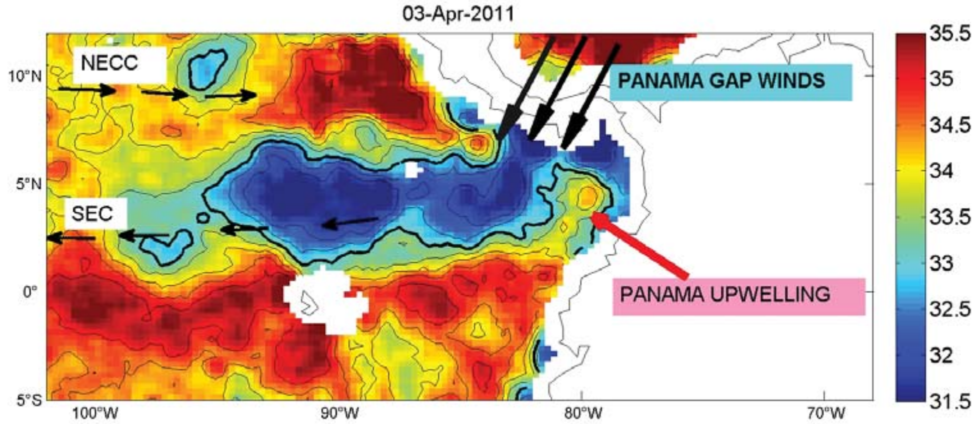

Figure 24: *10-days averaged SMOS SSS fields centered on the 28 Dec 2010 (Top), 16 Feb 2011 (middle) and 3 Apr 2011 (bottom). Small black arrows indicate the major surface currents, namely the South Equatorial Current (SEC) and North Equatorial Counter Current (NECC). Thick black contour is indicating the 32 isohaline.*

The lowest sea surface salinity (SSS) of the tropical Pacific Ocean, the Easter Pacific Fresh Pool (EPFP), is found between the warm pool characterized by a mean sea surface temperature (SST) greater than 28°C centered around 15°N along the coast of Central America and the cold and fresh equatorial region, with SSS values lower than 33 off the Panama isthmus and lower than 34 extending as far as130°W from the equator to 15°N (Figure 24).

The EPFP reflects both the conditions of excessprecipitation over evaporation beneath the ITCZ and inputsof fresh water from the Andes and Caribbean region (Benwayand Mix, 2004). Analysis of a recent gridded *in situ* SSS product (Delcroix et al., 2011) points out that interannual variations are relatively weak in the EPFP but that seasonal variations are the strongest within the tropical Pacific. Large-scale analysis suggests that the SSS seasonal balance is mostly driven by precipitation in the part of the EPFP covered by the ITCZ, but more complex in the far east as advection and entrainment become important processes (Bingham et al., 2010; Alory et al., 2012).

By focusing on seasonal SSS variations along a well-sampled Voluntary Observing Ship (VOS) line from Panama to Tahiti, Alory et al.(2012) recently showed that this fresh pool dynamically responds to strong regional ocean-atmosphere-land interactions. First, monsoon rains (and associated river runoff) give birth to the fresh pool inthe Panama Bight during summer and fall. Second, strong currents driven by topography-induced winds extend the poolwestward in winter while it eventually disappear by mixing with upwelled saltier waters to the east. These dynamic features also generate steep SSS fronts at the edges of the fresh pool (sometimes larger than ~4psu/° of longitude at the eastern edges).

These SSS fronts and the amplitude of their seasonal cycle are large enough to be detected by the new SMOS satellite mission. Compared to *in situ* data, SMOS satellite data provide a more homogeneous coverage with finer spatial resolution. Examples of SMOS SSS maps averaged over 10 days and centered at selected dates in December 2010, February and April 2011 are presented in Figure 24. Remarkably, all the major features observed with in situ VOS data as detailed in Alory et al. (2012) are well reproduced in the SMOS analysis, notably: the westward expansion of the fresh pool (SSS < 33) from 85°Win December to 95°W in April, the steep SSS front east of the 32 isohaline and SSS minimum of 28 in the Panama Bight in December, and the strong SSS increase to around 35 in the Panama Bight in April. Moreover, SSS changes occurring between December and April are qualitatively consistent with the expected effects of winter climatological currents, including the Panama Bight upwelling.

The freshwater pool disruption as observed by SMOS in the Panama bight (Figure 24, middle and bottom panels) are associated with the following processes: during the boreal winter, as the ITCZ moves southward, the north-easterly Panama gap wind creates a south-westward jet-like current in its path with a dipole of Ekman pumping/eddies on its flanks. As a result, upwelling in the Panama Bight brings cold and salty waters to the surface that erode the fresh pool on its eastern side while surface currents stretch the pool westward.

Interestingly, SMOS data are also able to detect other meso-scale features in the region around the fresh pool such as the near-equatorial SSS front or the local SSS maximum in the Costa Rica dome.

Therefore, SMOS SSS data will help in exploring qualitatively the seasonal dynamics of the fresh pools from their birth to their final erosion by wind-driven and turbulent processes (surface current stirring and wind-driven upwelling). Quantifying the relative contribution of the different mechanisms on SSS variations would require a model-based synergetic data analysis scheme to establish the mixed layer salt budget. Also, the regional occurrence of SSS fronts and barrier layers (de Boyer Montégut et al, 2007) suggests, by analogy with the western tropical Pacific, a link between surface and subsurface salinity which could give additional value to the satellite SSS data (Maes, 2008; Bosc et al., 2009). As barrier layers can play an active role on the tropical climate (e.g.,Maes et al., 2002, 2005), studying their impacts in the region seems worthwhile. This could be done through regional modeling combined with analysis of subsurface/surface *in situ* and satellite data. Also, interannual variations of the fresh pool, even if quantitatively smaller than its seasonal variations, need further investigation as ENSO is a strong climate driver in the eastern Pacific. Now that 3 years of SMOS data are available, such type of analysis can be initiated.

5.2Fresh Pools interactions with Tropical Cyclones

Because of the buoyant plume of fresh water that forms in the Atlantic due to discharge from the Amazon and Orinoco rivers, the North Western Tropical Atlantic (NWTA) region where the salt-driven upper ocean stratification may significantly impact ocean-atmosphere interactions under Tropical Cyclones. The spreading of the Amazon–Orinoco River plume exhibits a seasonal cycle coinciding with the Atlantic hurricane season (1 June through 30 November) with river influenced minimum salinities observed farthest eastward and north westward during the height of the hurricane season (mid-August to mid-October). As shown by Ffield, (2007), for the 1960 to 2000 time period, 60% and 68% of all category 4 and 5 hurricanes, respectively, passed directly over the likely plume region, revealing that the most destructive hurricanes may be influenced by plume–atmosphere interaction just prior to reaching the Caribbean. Historical *in situ* data reveal that average ocean surface temperatures first encountered by tropical cyclones moving westward between 12° and 20°N is only 26°C, but upon reaching the northern reaches of the Amazon–Orinoco River plume (e.g. see Figure 25), the average sea surface temperatures (SST) encountered by tropical cyclones are 2°C warmer. These warm ocean surface temperatures may play a role in hurricane maintenance and intensification since hurricanes can only form in extensive ocean areas with a surface temperature greater than 25.5 deg C (Dare and McBride, 2011). In addition, as shown by Ffield (2007), the buoyant, and therefore stable, 10- to 60-m-thick layer of the plume can mask the presence and influence of other ocean processes and features just below the plume, in particular cool (during hurricane season) surface temperatures carried by NBC rings. After shedding from the NBC retroflection, the 300–500-km-diameter anticyclonic (clockwise) NBC rings pass northwestward through the Amazon–Orinoco River plume toward the Caribbean. The limited observations reveal that at times the cool upper-layer temperatures of the NBC rings are exposed to the atmosphere while at other times they are hidden just underneath warm plume water. Strong winds from the 300–1000-km-diameter cyclonic (counterclockwise) hurricanes might quickly erode a thin plume, exposing several degrees-cooler NBC ring water to the surface, and potentially contributing to limit further development of hurricanes. As shown by Ffields (2007), the warm temperatures associated with the low-salinity Amazon–Orinoco River plume and the relatively cool temperatures associated with NBC rings are in close proximity to the passing hurricanes. As such they are expected to actively influence on the hurricane maintenance and intensification although the interaction is challenging to accurately quantify.

Vizzy and Cook (2010) more recently studied the atmospheric response of the summertime large scale climate to the Amazon/Orinoco plume sea surface temperature anomaly forcing using a regional climate model. They performed simulations in the presence or absence of the Amazon/Orinoco plume SST anomalies. Results from their simulations indicate that the plume does significantly influence the frequency and intensity of summertime storm systems over the Atlantic, consistent with Ffield (2007). The presence of the plume increases the average number of Atlantic basin storms per summer by 60%. An increase in storm intensity also occurs, with a 61% increase of the number of storms that reach tropical storm and hurricane strength. Results from their simulations suggests that Atlantic storms also tend to curve northward further west in the Atlantic basin in presence of the plume SST anomaly. These results support the premise that the warm and low salinity combined Amazon-Orinoco River plume play an important role in modulating the air-sea interaction during hurricane passages in a manner similar to persistent fresh water barriers layers.

For instance, when there is a fresh water barrier layer, such as in the North Western tropical Atlantic, mixing is restricted within shallower mixed layer and entrainment of cool thermocline water into the mixed layer is reduced (e.g., Anderson et al., 1996; Vialard and Delecluse,1998a,b; Foltz and McPhaden, 2009). As discussed in Price (2009), if the net salinity anomaly (fresh water layer thickness times salinity anomaly in the initial state) is as large as about 20 m, then the fresh layer will potentially inhibit vertical mixing significantly. As the fresh water surface layer (halocline) of the Amazon and Orinoco river plumes is warmer than the water below (Ffield, 2007), salinity stratification acts to reduce the depth of vertical mixing and thus sea surface cooling. The reduced cooling amplitude in the wake of hurricanes passing over the Amazon and Orinoco river plume, associated with thick BL effects, might be an important mechanism in favor of hurricane intensification in that region. Similar impact of barrier-layers on TC-induced sea surface cooling have been recently evidenced for several case studies such as in the Tropical Atlantic (Balaguru et al. 2012), in theBay of Bengal (Yu and McPhaden, 2011; Neethu et al., 2012) and in the tropical Northwest Pacific (Wang et al., 2011).

New insight into the interactions between such extreme atmospheric events and large-scale fresh pools at the ocean surface has been gained from the satellite based SSS observations as recently reported by Grodsky et al; (2012). They used data from the Aquarius/SAC-D and SMOS satellites to help elucidate the ocean response to hurricane Katia, which crossed the Amazon plume in early fall, 2011. As illustrated in their paper, the Katia passage left a 1.5 psu high haline wake covering >10^5 km^2 (in its impact on density, the equivalent of a 3.5°C cooling) due to mixing of the shallow BL.

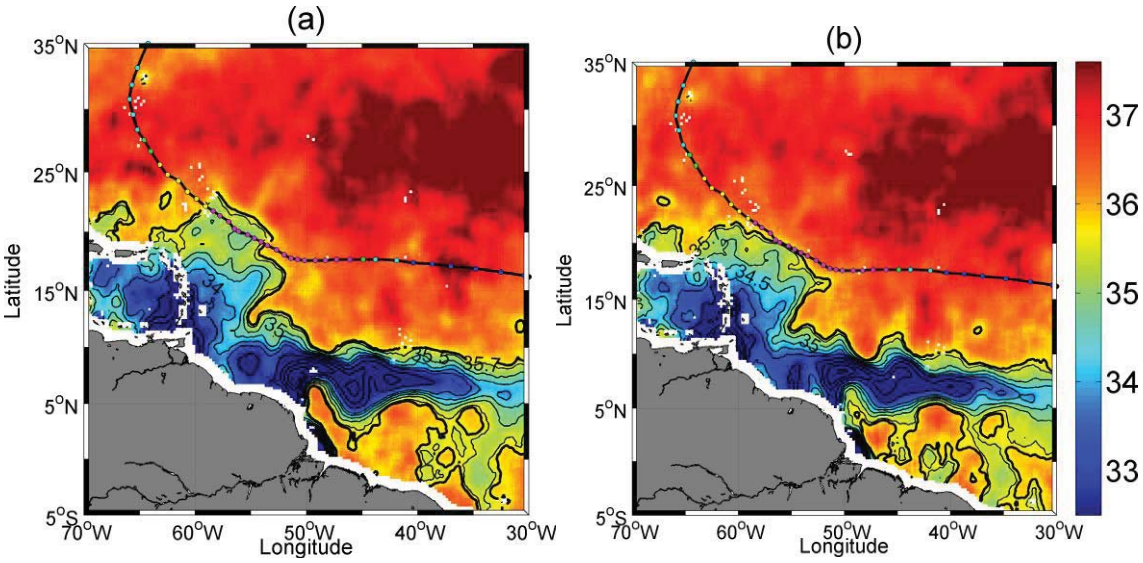

Figure 25: *Two SMOS microwave satellite-derived SSS composite images of the Amazon plume region revealing the SSS conditions (a) before and (b) after the passing of Hurricane Igor, a category 4 hurricane that attained wind speeds of 136 knots in September 2010 during its passage over the plume. Color-coded circles mark the successive hurricane eye positions. Seven days of data centered on (a) 10 Sep 2010 and (b) 22 Sep 2010 have been averaged to construct the SSS images, which are smoothed by a 1° x 1° block average.*

As illustrated in Figure 25, very similar observations were also detected from SMOS data alone during the passage of the Category 4 hurricane Igor over the river plume in 2010. The data evidence an erosion of the thin northern reach of the plume fresh surface layer by Igor hurricane-induced mixing, covering an area of ~89000 km^2 located on the storm right-hand side, where SSS increases by ~1 practical salinity unit whilst SST cools by 2-3°C. On the left side of the storm, much smaller SSS and SST changes are detected after the storm passage.The strong SSS increase in the hurricane wake within the plume is explained by the erosion of the BL. This is supported by Argo profiles collected within the plume (see Grodsky et al., 2012). Mixed layer salinity is lower by 2 to 4 psu than the water beneath. The shallow haline stratification is destroyed by hurricane-forced entrainment which is stronger on the right side of hurricane eye (Price, 2009). It results in a strong SSS signal. Although the hurricane strengthened further along the trajectory, the SSS change is much weaker there corresponding to weak vertical salinity stratification outside the plume. As further discussed in Grodsky et al., 2012, the fresh (more buoyant) BL limits the turbulent mixing and then the SST cooling in the plume, and thus preserved higher SST and fresh water evaporation than outside. Combined with SST, the new satellite SSS data thus provide a new and better tool to monitor the plume extent and quantify the upper ocean responses to tropical cyclones with important implications for hurricane forecasting.

6. Conclusions& Perspectives

The ocean is the primary return conduit for water transported by the atmosphere. It is the dominant element of the global water cycle, and clearly one of the most important components of the climate system, with more than 1100 times the heat capacity of the atmosphere. Two new satellite sensors, the ESA Soil Moisture and Ocean Salinity Mission (SMOS) and the NASA Aquarius SAC-D missions are now providing the first space borne measurements of the sea surface salinity (SSS). Synergetic analyses of the new surface salinity data sets together with sea surface temperature, dynamic height and surface geostrophic currents from altimetry, near surface wind, ocean color, in situ observations, and rainfall estimates will certainly help clarifying the fresh water budget in key oceanic tropical areas.

In this paper, we selected illustrative examples to review how the first SSS products derived from the SMOS sensor can readily help to better characterize some of the key processes of the marine branch of the global hydrological cycle. First, we illustrated the new monitoring capabilities for some of the world largest oceanic fresh water pools generated by the discharge of very large tropical rivers. In particular, we show how SMOS SSS traces the fresh water signals from the Amazon-Orinoco and Congo river plumes.River runoff is an important variable in oceanography as their fresh water affects SSS and the buoyancy of the surface layer, and they represent a source of materials exotic to the ocean and highly important to biological activity. Obviously, they are key hydrologic components of the fresh water exchanges between the atmosphere, land and ocean. Despite this importance, tracing river fresh watertransport over large distances has not been straightforward previously principally because of a lack of SSS data. Tracing those very large rivers over great distances now become an important endeavor, as sufficient data are available from the SMOS and Aquarius sensors that can be further combined with satellite derived surface geostrophic current data.

Second, we evidenced key oceanic precipitation signatures in the SMOS SSS signal. Satellite radiometry at L-band provides for the first time a global measure of the salinity at the ocean-atmosphere interface (within the upper centimeters). Rain events induce freshening of the ocean surface and are responsible for a high temporal variability in the SSS, consistently detected by both *in situ* and spaceborne sensors. Because of the vertical haline gradient generated by the rain-induced freshening in the upper ocean, fresher surface waters are however systematically found from space in rainy area compared with the 1-10 m depth in situ data. These differences challenge calibration/validation activities of the satellite SSS in high precipitation regions. Nevertheless, satellite SSS data certainly provide new information about ocean-atmosphere interfacial fresh water fluxes in these conditions. This was evidenced by comparing spatial patterns and amplitudes of the large scale SSS anomalies estimated from the SMOS data and the net Evaporation minus Precipitation fluxes in the Tropical Atlantic. Under the InterTropical Convergence Zone and sufficiently far away from the river runoff signals, residual SSS anomalies were shown to be highly correlated to the *E-P* anomalies. In particular, SSS anomalies become increasingly negative as the Precipitation anomalies progressively exceed the Evaporation anomalies. This demonstrate the importance of monitoring SSS from space in rainy regions, suggesting that the interfacial SSS values might be a good large-scale oceanic rain gauge of the global hydrological water cycle.

The interfacial character of the spaceborne measurements also offer new information of interest for ocean circulation models in the perspective of better constraining oceanic precipitation forcing terms.

Finally, the SSS observations from SMOS satellite were used to reveal new aspect of the main tropical fresh pool evolution and interaction with wind-driven atmospheric processes. SMOS imagery thus captures how the large Eastern Pacific Fresh Pool is systematically eroded at the end of the boreal summer on its eastern side by the wind-driven Panama Upwelling which brings cold and salty waters to the surface. Prior to SMOS data availability, the few existing studies of the eastern Pacific describing seasonal variations of SSS did not investigate their cause beyond rainfall (e.g., Fiedler and Talley, 2006). Thanks to the new SMOS data, SSS variability associated with wind-driven processes in that region, such as the Panama upwelling signal recently evidenced by Alory et al. (2012), can now be characterized more deeply.

Because of the buoyant character of the fresh water that forms at the ocean surface due to large river discharges or intense local precipitation, the upper ocean stratification in several key tropical oceans regions (e.g., North Western Tropical Atlantic, Eastern and Western Pacific Fresh Pools, Bay of Bengal) is mostly controlled by salinity. In such freshwater pool regions, a uniform density mixed layer is found to form the so-called Barrier Layers at shallower depth than the uniform temperature layer. Because of stable halocline, the BL are acting to inhibit surface cooling and vertical mixing under the action of surface wind stresses. Therefore, there can be some feedback mechanisms between atmospheric, or terrestrial, fresh water fluxes to the ocean and intense atmospheric processes. About 68% of hurricanes that finally reached category 4 and 5 have thus crossed the Amazon/Orinoco plume [Ffield, 2007] where the presence of Barrier Layers can enhance their growth rate by 50% [Balaguru et al., 2012]. Under an intense hurricane, the halocline, which is above the thermocline, is first mixed. This produces a SSS wake that is by a few psu saltier than initial SSS in the plume. By analysing SMOS SSS data before and after the passage of several intense hurricanes over the Amazon river plume in 2010 and 2011, SSS changes >1 psu over areas exceeding 10^5 km^2 were detected. These abrupt changes have implications for SSS climate, since SSS is more long-lived and not damped like SST. In addition, destruction of the BL is apparently associated with a decreased SST cooling in the plume that, in turn, preserves higher SST and evaporation than outside the BL. This difference in SST cooling is explained by additional work required to mix the BL. Thus BL leads to a reduction in hurricane-induced surface cooling that favors hurricane intensification, as the resulting elevated SST and high evaporation enhance the hurricane's maximum potential intensity. The geographic location and seasonality of the Amazon/Orinoco plume make hurricane overpasses a frequent occurrence. Indeed, the expansion of the plume in August-September coincides with the peak of the production of Cape Verde hurricanes, which includes many of the most intense (Category 4–5) hurricanes. Thus the results presented here strongly suggest that the role of the salinity stratification in mixed layer dynamics should be taken into account when forecasting tropical cyclone growth over freshwater pools that are generating thick BL (Amazon plume, Bay of Bengal, Eastern and Western Pacific Fresh Pools). The availability of satellite SSS from Aquarius and SMOS along with in situ Argo measurements is critical to making such model improvements practical.

Acknowledgements

Work presented in this paper was partly done under ESA support in the context of the development of the SMOS Level 2/Expert Support Laboratory, ESA Support to Science Element SMOS+SOS and SMOS+STORM projects. CNES also partly funded these activities in the frame of the Centre Aval de Traitement des Données SMOS (CATDS) and of the SMOS/ESA GLOSCAL Cal/Val projects. We are indebted to Micha Rijkenberg (Koninklijk Nederlands Instituut voor Onderzoek der Zee · Department of Biological Oceanography (BIO)) for giving us access to the Geotraces Leg 2 CTD data, to F. Gaillard (LPO/IFREMER) for providing ISAS maps version 6 (see *http://wwz.ifremer.fr/lpo/SO-Argo/Products/Global-Ocean-T-S*). Gilles Reverdin (LOCEAN/CNRS) is responsible for french salinity drifter deployment program, he supervised the quality control of these drifter data set and is warmly acknowledged. These data are available on www.locean-ipsl.upmc.fr/smos/drifters. We thank Nicolas Martin for data processing. We are also indebted to JéromeVialard, MatthieuLengaigneand Emmanuel Vincent for their very helpful comments about SSS variability in the tropical Indian Ocean and about Tropical Cyclones interactions with the Amazon plume, Thierry Delcroix about SSS variability in the tropical Pacific Ocean. SSM/I data have been processed by Remote Sensing System (www.ssmi.com). The global ocean heat flux and evaporation products were provided by the WHOI OAFlux project (http://oaflux.whoi.edu) funded by the NOAA Climate Observations and Monitoring (COM) program.

References

Alory G, Maes C, Delcroix T, Reul N, Illig S (2012), Seasonal dynamics of sea surface salinity off Panama: the far eastern Pacific fresh pool, J. Geophys. Res. 117: C04028

Anderson SP, Weller RA, Lukas R (1996) Surface Buoyancy Forcing and the Mixed Layer of the Western Pacific Warm Pool: Observations and 1D Model Results. J. Climate, **9**, 3056–3085

Baklouti M, Devenon JL, Bourret A, Froidefond JM, Ternon JF, Fuda JL (2007) New insights in the French Guiana continental shelf circulation and its relation to the North Brazil Current retroflection, J. Geophys. Res. 112: C02023

Balaguru KP, Saravanan SR, Leung LR, Xu Z, Li M, Hsieh JS, (2012) Ocean barrier layers' effect on tropical cyclone intensification, *PNAS*, doi:10.1073/pnas.1201364109

Banks CJ, Gommenginger CP, Srokosz MA., Snaith HM (2012) Validating SMOS ocean surface salinity in the atlantic with Argo and operational ocean model data, IEEE Transactions on Geoscience and Remote Sensing 50: 1688–1702

Benway HM, Mix AC (2004) Oxygen isotopes, upper-ocean salinity, and precipitation sources in the eastern tropical Pacific, Earth Planet. Sci. Lett., 224: 493–507

Binet D, Marchal E (1993) The Large Marine Ecosystem of Shelf Areas in the Gulf of Guinea:Long-Term Variability Induced by Climatic Changes. In Kenneth Sherman, et al. (eds.), Large Marine Ecosystems: Stress, Mitigation, and Sustainability (Washington, D.C.: American Association for the Advancement of Science, 1993) : 104-118.

Bingham FM, Foltz GR, McPhaden MJ (2010), Seasonal cycles of surface layer salinity in the Pacific Ocean, Ocean Sci., 6: 775–787

Blough NV, Del Vecchio R (2002), Chromophoric DOM in the coastal environment, in Biogeochemistry of Marine Dissolved Organic Matter, edited by D. A. Hansell, and C. A. Carlson, pp. 509–546, Academic, San Diego, Calif

Bonjean F, Lagerloef GSE (2002): Diagnostic Model and Analysis of the Surface Currents in the Tropical Pacific Ocean. J. Phys. Oceanogr. (32): 2938–2954

Bornhold BD (1973) Late Quaternary sedimentation in the eastern Angola Basin. Massachusetts Institute of Technology: 1-213 (thesis).

Bosc C, Delcroix T, Maes C (2009) Barrier layer variability in the western Pacific warm pool from 2000 to 2007, J. Geophys. Res., 114, C06023

Boutin J, Martin N, Yin X, Reul N, Spurgeon P (2012a) First Assessment of SMOS Data Over Open Ocean: Part II-Sea Surface Salinity. IEEE Transactions on Geoscience and Remote Sensing 50 (5) Part 1: 1662 - 1675

BoutinJ, Martin N, Reverdin G, Yin X, Gaillard F (2012b), Sea surface freshening inferred from SMOS and Argo salinity: Impact of rain, Ocean Sci. Discuss., 9, 3331-3357

Boyer TP, Levitus S (2002) Harmonic analysis of climatological sea surface salinity, J. Geophys. Res., 107(C12): 8006

Braga ES, Andrie C, Bourles B, Vangriesheim A, Baurand F, Chuchla R (2004) Congo River signature and deep circulation in the eastern Guinea Basin. Deep Sea Research Part I:Oceanographic Research Papers 51 (8): 1057-1073.

Carval T, Keeley B, Takatsuki Y, Yoshida T, Loch S, Schmid, C, Goldsmith R, Wong A, McCreadie R, Thresher A, Tran A (2012) Argo User's Manual v2.4, 85, IFREMER referencecor-do/dti-mut/02-084

Cherubin LM, Richardson PL (2007) Caribbean Current Variability And The Influence Of The Amazon And Orinoco Freshwater Plumes, Deep-Sea Research Part I-Oceanographic Research Papers, 54(9): 1451-1473

Conmy RN, Coble PG, Cannizzaro JP, Heil CA (2009) Influence of extreme storm events on West Florida Shelf CDOM distributions, J. Geophys. Res., 114, G00F04

Cravatte S, Delcroix T, Zhang D, McPhaden MJ, Leloup J (2009). Observed freshening and warming of the western Pacific warm pool.Clim. Dyn. 33, 565–589

Dare RA., McBride JL(2011) The Threshold Sea Surface Temperature Condition for Tropical Cyclogenesis. J. Climate, 24: 4570–4576.

Del Vecchio R, Subramaniam A (2004) Influence of the Amazon River on the surface optical properties of the Western Tropical North Atlantic Ocean, J. Geophys. Res., 109, C11001

De Boyer Montégut C,MignotJ, Lazar A, CravatteS (2007), Control of salinity on the mixed layer depth in the world ocean: 1. General description, J. Geophys. Res., 112, C06011

Delcroix T, Alory G, Cravatte S, Corrège T, McPhaden MJ (2011) A gridded sea surface salinity data set for the tropical Pacific with sample applications (1950–2008), Deep Sea Res., Part I 58(1): 38–48

DeMaster D J, Smith W, Nelson DM, Aller JY (1996), Biogeochemical processes in Amazon shelf waters: Chemical distributions and uptake rates of silicon, carbon and nitrogen, Cont. Shelf Res., 16: 617–643

Dessier A, Donguy J (1994) The Sea-Surface Salinity In The Tropical Atlantic Between 10-Degrees-S And 30-Degrees-N - Seasonal And Interannual Variations (1977-1989), Deep-Sea Research Part I-Oceanographic Research Papers, 41(1): 81-100

Dickson RR, Yashayaev I, Meincke J, Turrell W, Dye S, Holfort J (2002) Rapid freshening of the deep North Atlantic Ocean over the past four decades. Nature 416: 832-837

Donguy JR, Hénin C (1980) Surface conditions in the eastern equatorial Pacific related to the intertropical convergence zone of the winds, Deep Sea Res., Part A, 27: 693–714

D'Sa EJ, Hu C, Muller-Karger FE, Carder KL (2002) Estimation of colored dissolved organicmatter and salinity fields in case 2 waters using SeaWiFS: Examples from Florida Bay and Florida Shelf, J. Earth Syst. Sci., 111: 197–207

Durack PJ, Wijffels SE, Matear RJ (2012) Ocean salinities reveal strong global water cycle intensification during 1950 to 2000, Science 336: 455–458

Eisma D, Van Bennekom A.J. (1978) The Zaire river and estuary and the Zaire outflow in the Atlantic ocean. Netherlands Journal of Sea Research 12 (3/4), 255–272.

Ferrari GM, Dowell MD (1998) CDOM absorption characteristics with relation to fluorescence and salinity in coastal areas of the southern Baltic Sea, Estuarine Coastal Shelf Sci., 47, 91–105

FfieldA (2005) North Brazil Current rings viewed by TRMM Microwave Imager SST and the influence of the Amazon Plume. Deep-Sea Res. I, 52: 137–160

Ffield A, (2007) Amazon and Orinoco River plumes and NBC Rings: bystanders or participants in hurricane events? J. Clim. 20: 316-333

Fiedler PC, Talley LD (2006), Hydrography of the eastern tropical Pacific: A review, Prog. Oceanogr., 69(2–4): 143–180

Flagg CN, Gordon RL, McDowell S (1986) Hydrographic and current observations on the continental slope and shelf of the western equatorial atlantic, Journal of Physical Oceanography 16(8): 1412-1429

Foltz GR, McPhaden JM (2009) Impact of barrier layer thickness on SST in the central tropical North Atlantic. J. Climate 22: 285-299

Font J, Camps A, Borges A, Martín-Neira M, Boutin J, Reul N, Kerr YH, Hahne A, Mecklenburg S (2010) SMOS: The Challenging Sea Surface Salinity Measurement from Space, Proceedings of the IEEE 98(5):649-665

Font J, Boutin J, Reul N, Spurgeon P, Ballabrera-Poy J, Chuprin A, Gabarró C, Gourrion J, Guimbard S, Hénocq C, Lavender S, Martin N, Martínez J, McCulloch M, Meirold-Mautner I, Mugerin C, Petitcolin F, Portabella M, Sabia R, Talone M, Tenerelli J, Turiel A, Vergely JL, Waldteufel P, Yin X, Zine X, Delwart S (2013) SMOS first data analysis for sea surface salinity determination, International Journal of Remote Sensing, DOI:10.1080/01431161.2012.716541

Froelich PN, Atwood DK, Giese GS (1978) Influence of amazon river discharge on surface salinity and dissolved silicate concentration in the caribbean sea, Deep Sea Research,25(8):735-744

Gaillard F, Autret E, Thierry V, Galaup P, Coatanoan C, Loubrieu T (2009) Quality control oflarge Argo datasets, J. Atmos. Ocean. Tech., 26, 337–351

Garzoli SL, Ffield A, Johns WE, Yao Q (2004) North Brazil Current retroflection and transports, J. Geophys. Res., 109, C01013

Goni GJ, Johns W (2001) A Census of North Brazil Current Rings Observed from T/P Altimetry: 1992-1998, Geophys. Res. Let., 1-4

Gordon A, Guilivi CF (2008) Sea surface salinity trends over 50 years within the subtropicalNorth Atlantic. Oceanography 20 (1): 20-29

Gouriou Y, Delcroix T (2002) Seasonal and ENSO variations of sea surface salinity and temperature in the South Pacific Convergence Zone during 1976–2000. Journal of Geophysical Research 107: 3185

Grodsky SA, Reul N, Lagerloef G, Reverdin G, Carton JA, Chapron B, Quilfen Y, Kudryavtsev VN, Kao HY (2012) Haline hurricane wake in the Amazon/Orinoco plume: AQUARIUS/SACD and SMOS observations, Geophys. Res. Lett., 39, L20603

Grunseich G, Subrahmanyam B, Murty VSN, Giese BS (2011) Sea surface salinity variability during the Indian Ocean Dipole and ENSO events in the tropical Indian Ocean, J. Geophys. Res., 116: C11013

Hellerman S, Rosenstein M (1983), Normal monthly wind stress over the world ocean with error-estimates, Journal Of Physical Oceanography, 13(7): 1093-1104

Hellweger F, Gordon A (2002), Tracing Amazon River water into the Caribbean Sea, Journalof Marine Research, 60 : 537-549

Hisard P, (1980) Observation de réponses de type "El Niño" dans l'Atlantique tropical oriental, Golfe de Guinée. Oceanol.Acta 3: 69-78

Hu C, Montgomery ET, Schmitt RW, Muller-Karger FE (2004) The dispersal of the Amazonand Orinoco River water in the tropical Atlantic and Caribbean Sea: Observation from space and S-PALACE floats, Deep Sea Res. Part II, 51: 1151–1171.

Johns, WE, Lee TN, Schott FA, Zantopp RJ, Evans RH (1990) The north brazil current retroflection: Seasonal structure and eddy variability, J. Geophys. Res. 95: 22103-22120

Katsaros KB, Buettner K JK (1969) Influence of Rainfall on Temperature and Salinity at the Ocean Surface, J. Appl. Meteorol. 8: 15–18.

Kerr Y, Waldteufel P, Wigneron JP, Delwart S, Cabot F, Boutin J, Escorihuela MJ, Font J, Reul N, Gruhier C (2010) The SMOS Mission: New Tool for Monitoring Key Elements of the Global Water Cycle. Proceedings of the IEEE 98(5): 666-687

Klein LA, Swift CT (1977) Improved model for dielectric constant of seawater at microwavefrequencies.IEEE Transactions on Antennas andPropagation 25: 104-111.

Koleshnikov AG (1973) Equalant I and Equalant II, Physical oceanography. UNESCO, Paris 1: 1-289

Lagerloef GSE, Mitchum G, Lukas R, Niiler P (1999) Tropical Pacific near surface currentsestimated from altimeter, wind and drifter data. J. Geophys. Res., 104: 23,313-23,326

Lagerloef GSE, Colomb FR, Le Vine D, Wentz F, Yueh S, Ruf C, Lilly J, Gunn J, Chao Y, deCharon A, Feldman G, Swift C (2008) The Aquarius/SAC-D Mission: Designed to meet the salinity remote-sensing challenge. Oceanography 21(1):68–81

Lagerloef GSE, Boutin J, Chao Y, Delcroix T, Font J, Niiler P, Reul N, Riser S, Schmitt R, Stammer D, Wentz F (2010) Resolving the Global Surface Salinity Field and Variations by Blending Satellite and In Situ Observations, Oceanobs'09: Sustained Ocean Observations and Information for Society, Venise, Italy, 21–25 September 2009, ESA Publication WPP-306

Lagerloef GSE (2012) Satellite mission monitors ocean surface salinity, Eos Trans. AGU 93(25), 233, doi:10.1029/2012EO250001.

Lefèvre N (2009) Low C02 concentrations in the gulf of guinea during the upwelling season in 2006, Marine Chemistry, 113(1-2), 93

Lentz SJ (1995) Seasonal-Variations In The Horizontal Structure Of The Amazon Plume Inferred From Historical Hydrographic Data, J. Geophys. Res., 100(C2): 2391-2400

Lentz SJ, Limeburner R (1995) The Amazon River Plume during AMASSEDS: Spatial characteristics and salinity variability, J. Geophys. Res., 100: 2355–2375

Maes C (2008) On the ocean salinity stratification observed at the eastern edge of the equatorial Pacific warm pool, J. Geophys. Res., 113, C03027

Maes C, Picaut J, Belamari S (2002) Salinity barrier layer and onset of El Niño in a Pacific coupled model, Geophys. Res. Lett., 29(24), 2206

Maes C, Picaut J, Belamari S (2005), Importance of salinity barrier layer for the buildup of El Niño, J. Clim., 18, 104–118

Meade RH, Nordin CF, Hernandez DP, Mejia A, Godoy JMP (1983) Sediment and water discharge in Rio Orinoco,Venezuela and Colombia. In: Proceedings of the Second International Symposium on River Sedimentation. Water resourcesand Electric Poers Press, Beijing, China, pp. 1134–1144.

Mecklenburg S, Drusch M, Kerr YH, Font J, Martin-Neira M, Delwart S, Buenadicha G, Reul N, Daganzo-Eusebio E, Oliva R, Crapolicchio R (2012) ESA's Soil Moisture and Ocean Salinity Mission: Mission Performance and Operations, IEEE Transactions on Geoscience and Remote Sensing 50 (5) Part 1: 1354 - 1366

Merle J, (1980) Variabilité thermique annuelle et interannuelle de l'océan Atlantique équatorial est. L'hypothèse d'un " El Niño " Atlantique. Oceanol. Acta 3, 209-220

Meulenbergh J (1968) Diffusion des eaux du fleuve Congo dans les eaux de l'Atlantique Sud.Acad. roy. SC. Outre-Mer, SC. Te&., N.S. SVI (6) Bruxelles, 148 p.

Meybeck M, Ragu A (1997) River discharges to the oceans: An assessment of suspended solids, major ions, and nutrients, IAHS Publ., 243: 1–245

Michel S, Chapron B, Tournadre J, Reul N (2007) Sea surface salinity variability from a simplified mixed layer model of the global ocean, Ocean Sci. Discuss., 4: 41–106

Mignot J, de Boyer Montégut C, Lazar A, Cravatte S (2007) Control of salinity on the mixed layer depth in the world ocean: 2. Tropical areas. J. Geophys. Res., 112, C10010

Miller R, Zepp RG (1995) Photochemical production of dissolved inorganic carbon from terrestrial organic matter: Significance to the oceanic organic carbon cycle, Geophys.Res. Lett., 22, 417–420

Milliman JD, Meade RH (1983) World-wide delivery of river sediment to the oceans, The Journal of Geology, 91(1): 1-21

Molleri GSF, de M. Novo EML, Kampel M (2010), Space-time variability of the Amazon River plume based on satellite ocean color, Continental Shelf Research 30(3–4):, 342-352

Moran M A, Sheldon WM, Sheldon JE (1999), Biodegradation of riverine dissolved organiccarbon in five estuaries of the southeastern United States, Estuaries, 22: 55–64

Morrow R, Valladeau G, Sallee J-B (2008) Observed subsurface signature of Southern Ocean sea level rise. Prog.Oceanogr. 77(4): 351–366

Muller-Karger FE, McClain CR, Richardson PL (1988) The dispersal of the Amazon's water, Nature, 333 : 56–59

Muller-Karger FE, McClain CR, Fisher TR, Esaias WE, Varela R(1989) Pigment distribution in the Caribbean Sea: Observations from space, Prog. Oceanogr., 23: 23–64

Muller-Karger FE, Richardson PL, McGillicuddy D (1995), On the offshore dispersal of the Amazon's Plume in the North Atlantic, Deep Sea Res. Part I, 42: 2127–2137

Neetu S, Lengaigne M, Vincent EM, Vialard J, Madec G, Samson G,Ramesh Kumar MR, Durand F (2012) Influence of upper-ocean stratification on tropical cyclones-induced surface cooling in the Bay of Bengal. Journal of Geophysical Research, 117, C12020

Neumann G (1969) Seasonal salinity variations in the upper strata of the western tropical Atlantic ocean-I. Sea surface salinities, Deep-Sea Res. 16: 165-177

Nittrouer CA, Demaster DJ (1986), Sedimentary processes on the Amazon continental shelf: past, present and future research, Continental Shelf Research, 6: 5-30

Obernosterer I, Herndl GJ (2000) Differences in the optical and biological reactivity of the humic and non-humic DOC component in two contrasting coastal marine environments, Limnol. Oceanogr., 45: 1120–1129

Ostapoff F, Tarbeyev Y, Worthem S (1973) Heat Flux and Precipitation Estimates from Oceanographic Observations, Science 180: 960–962.

Palacios SL, Peterson TD, Kudela RM (2009), Development of synthetic salinity from remote sensing for the Columbia River Plume, J. Geophys. Res., 114: C00B05

Perry GD, Duffy PB, Miller NL (1996) An extended data set of river discharges for validation of general circulation models, J. Geophys. Res. 101: 21339-21349

Piterbarg LI, Ostrovskii AG(1997) Advection and Diffusion in Random Media: Implications for Sea Surface Temperature Anomalies. Kluwer Academic, 330 pp.

Piton B, Wacongne S (1985). Unusual amounts of very saline subsurface water in the eastern Gulf of Guinea in May 1984. Tropical Ocean-Amosphere Newsletter 325-8

Price JF (2009) Metrics of hurricane-ocean interaction: Vertically-integrated or vertically-averaged ocean temperature? Ocean Science 5:351–368.

Reul N, Saux-Picart S, Chapron B, Vandemark D, Tournadre J, Salisbury J (2009), Demonstration of ocean surface salinity microwave measurements from space using AMSR-E over the Amazon plume, Geophys. Res. Letters, 36, L13607

Reul, N, Tenerelli J (2011) SMOS Level 3 SSS Research products - Product Validation Document - Reprocessed Year 2010. CECOS/CNES/IFREMER/CATDS Techn Doc (available from www.catds.fr).

Reul N, Tenerelli J, Boutin J, Chapron B, Paul F, Brion E, Gaillard F, Archer O (2012) Overview of the First SMOS Sea Surface Salinity Products. Part I: Quality

Assessment for the Second Half of 2010. IEEE Transactions on Geoscience and Remote Sensing 50 (5) : 1636 - 1647

Reverdin G, Kestenare E, Frankignoul C, Delcroix T (2007), Sea surface salinity in the Atlantic Ocean (30°S–50°N), Prog. Oceanogr., 73: 311–340

Reverdin G, Morisset S, Boutin J, Martin N (2012) Rain-induced variability of near sea-surface *T* and *S* from drifter data, J. Geophys. Res., 117, C02032

Richardson PL, McKee T (1984) Average seasonal variation of the atlantic equatorial currents from historical ship drifts, Journal of Physical Oceanography, 14(7):1226-1238

Ruf CS, Swift CT, Tanner AB, Le Vine DM(1988)Interferometric synthetic aperture microwave radiometry for the remote sensing of the Earth.*IEEE Transactions on Geoscience and Remote Sensing*, 26, pp. 597-611.

Salisbury J, Vandemark D, Campbell J, Hunt C, Wisser D, Reul N, Chapron B (2011) Spatial and temporal coherence between Amazon River discharge, salinity, and light absorption by colored organic carbon in western tropical Atlantic surface waters, J.Geophys. Res., 116, C00H02

Schlössel P, Soloviev A, Emery WJ (1997) Cool and freshwater skin of the ocean during rainfall, Boundary-Layer Meteorology 82 (3): 439-474

Schmitt RW(2008) Salinity and the global water cycle, Oceanography 21(1):12–19

Singh A, Delcroix T, Cravatte S (2011) Contrasting the flavors of El Niño-Southern Oscillation using sea surface salinity observations, J. Geophys. Res., 116: C06016

Smith WO, Demaster DJ (1996) Phytoplankton biomass and productivity in the amazon river plume: correlation with seasonal river discharge, Continental Shelf Research, 16(3):291-319

Soloviev A, Lukas R (1996) Observation of spatial variability of diurnal thermocline and rainformed halocline in the Western Pacific warm pool, J. Phys. Oceanogr., 26: 2529– 2538

Steven DM, Brooks AL (1972), Identification of amazon river water at barbados, w. indies, by salinity and silicate measurements, Marine Biology, 14(4): 345-348

Ternon, JF, Oudot C, Dessier A, Diverres D (2000) A seasonal tropical sink for atmospheric $C0_2$ in the atlantic ocean: the role of the amazon river discharge, Marine Chemistry 68(3): 183-201

Terray L, Corre L, Cravatte S, Delcroix T, Reverdin G, Ribes A. (2011) Near-surface salinityas nature's rain gauge to detect human influence on the tropical water cycle, J. Climate, 25:958–977

Twardowski MS, Donaghay PL (2001) Separating in situ and terrigenous sources of absorption by dissolved material in coastal waters, J. Geophys. Res., 106(C2): 2545– 2560

UNESCO: The international system of units (SI) in oceanography, UNESCO Technical Papers No. 45, IAPSO Pub. Sci. No. 32, Paris, France, 1985.

Van Bennekom AJ, JagerJE (1978) Dissolved aluminium in the Zaire river plume, Neth. J.Sea Res. 12 (3/4): 358-367.

Van Bennekom AJ, Berger GW (1984), Hydrography and silica Budget of the Angola Basin, Netherlands Journal of Sea Research 17 (2-4): 149-200

Vangriesheim A, Pierre C, Aminot A, Metzl N, Baurand F, Caprais JC (2009) The influence of Congo river discharges in the surface and deep layers of the gulf of guinea, Deep Sea Re- search Part II: Topical Studies in Oceanography56(23): 2183-2196

Vialard J, Delecluse P (1998a) An OGCM Study for the TOGA Decade. Part I : Role of Salinity in the Physics of the Western Pacific Fresh Pool. Journal of Physical Oceanography, 28: 1071 - 1088

Vialard J, Delecluse P (1998b) An OGCM Study for the TOGA Decade. Part II : Barrier Layer Formation and Variability. Journal of Physical Oceanography, 28:1089 -1106

Vizy EK, Cook KH (2010) Influence of the Amazon/Orinoco Plume on the summertime Atlantic climate, J. Geophys. Res., 115, D21112

Vörösmarty CJ, Fekete B, Tucker BA(1998) River dischargeDatabase, Version 1.1 (RivDIS v1.0 supplement). Institute forthe Study of Earth, Oceans, and Space, University of NewHampshire, Durham, NH

Wang X, Han G, Qi, Y, Li W (2011) Impact of barrier layer on typhoon-induced sea surfacecooling, Dynamics of Atmospheres and Oceans, 52, 3: 367-385

Wauthy B (1977) - Révision de la classification des eaux de surface du golfe de Guinée. Cah.O.R.S.T.O.M., sér.Océanogr., 15 (3) : 279-295.

Wijesekera HW, Paulson CA, Huyer A (1999) The effect of rainfall onthe surface layer during a westerly wind burst in the western equatorialPacific, J. Phys. Oceanogr., 29: 612– 632

Wisser D, Fekete BM, Vörösmarty CJ, Schumann AH (2010) Reconstructing 20th century global hydrography: A contribution to the Global Terrestrial Network-Hydrology (GTN-H), Hydrol. Earth Syst. Sci., 14: 1–24

Yamashita Y, Tanoue E (2004), In situ production of chromophoric dissolved organic matter in coastal environments, Geophys. Res. Lett. 31: L14302

Yin X, Boutin J, Martin N, Spurgeon P (2012) Optimization of L-Band Sea Surface Emissivity Models Deduced From SMOS Data, IEEE Transactions on Geoscience and Remote Sensing 50: 1414-1426

Yoo JM, Carton JA (1988), Spatial Dependence of the Relationship between Rainfall and Outgoing Longwave Radiation in the Tropical Atlantic., Journal of Climate, 1: 1047- 1056

Yu L, Weller RA (2007) Objectively Analyzed air-sea heat Fluxes (OAFlux) for the global ocean, Bull. Am. Meteorol. Soc., 88(4): 527–539

Yu L (2010) On Sea Surface Salinity Skin Effect Induced by Evaporation and Implications for Remote Sensing of Ocean Salinity, Journal of Physical Oceanography 40 (1) 85

Yu L (2011) A global relashionship between the ocean water cycle and near-surface salinity,Journal of geophysical Research, 116: C10025

Yu L, McPhaden MJ (2011) Ocean pre-conditioning of Cyclone Nargis in the Bay of Bengal:Interaction between Rossby waves, surface fresh waters, and sea surface temperatures. J. Phys. Oceanogr., 41, 1741-1755.

Yueh SH, West R, Wilson WJ, Li FK, Njoku EG, Rahmatsamii Y (2001), Error sources and feasibility for microwave remote sensing of ocean surface salinity. IEEE Transactionson Geoscience and Remote Sensing, 39: 1049-1060

Zhang Y, Zhang X (2012) Ocean haline skin layer and turbulent surface convections, J. Geophys. Res., 117, C04017